Rheinland-Pfälzische Technische Universität Kaiserslautern Landau

RPTU Center for Cognitive Science

IBB Institute for Biomagnetism and Biosignalanalysis

Universität Münster

Machine-learning spike marking in Signal and Source space
Maschinelles Lernen zur Markierung von Spikes im Signal- und Quellenraum

Lala Jafarova

A THESIS PRESENTED FOR THE DEGREE OF MASTER OF SCIENCE IN COGNITIVE SCIENCE

by
Name: Lala Jafarova
Matriculation Number: 425736

supervised by: Prof. Dr. rer. nat. Carsten Wolters
apl. Prof. Dr. Daniela Czernochowski

Submitted on: August 20, 2025

Declaration of Authorship

I hereby declare that the work presented here is, to the best of my knowledge and belief, original and the result of my own investigations, except as acknowledged, and has not been submitted, either in part or whole, for a degree at this or any other university.

_____

signature

_____

date, city

Acknowledgements

I would like to express my sincere gratitude to all individuals who contributed to the successful completion of this research.

First and foremost, I extend my deepest appreciation to my supervisor, Prof. Dr rer. nat. Carsten Wolters, for his invaluable guidance, support, insightful discussions and continuous encouragement throughout this project. His expertise and dedication were instrumental in shaping this work.

I am also grateful to my co-supervisor, Apl. Prof. Dr Daniela Czernochowski from the Cognitive Neuroscience group, RPTU Kaiserslautern, as well as to my fellow researchers, especially Demet Yeşilbaş from the Department of Biomedical Engineering, Graduate School of Natural and Applied Sciences, Erciyes University, and Yvonne Buschermöhle and Malte Höltershinken from Prof. Wolters' SIM-NEURO work-group at the Institute for Biomagnetism and Biosignalanalysis, University of Münster, for their constructive discussions and supportive research environment they fostered.

This work was supported by ERA PerMed as project ERAPERMED2020-227, PerEpi (Bundesministerium für Gesundheit (BMG), project ZMI1-2521FSB006), by the Deutsche Forschungsgemeinschaft (DFG), projects WO1425/10-2 and WO1425/11-1, and by DAAD project 57756407.

Finally, I wish to thank my family and friends who supported me in this journey.

Abstract

Accurate detection of interictal epileptiform discharges (IEDs) in electroencephalography (EEG) plays a crucial role in epilepsy diagnosis. This thesis investigates the classification of IEDs using Artificial Neural Networks (ANNs) trained on EEG data represented in both signal and source space. Source waveforms were computed using equivalent current dipole models fitted to averaged IED. Two source modeling approaches were evaluated: a 1-parameter fixed-orientation dipole and a 3-parameter projection, both localized to a single best-fit position during the rising flank of the IED.

ANN was trained on raw and feature-extracted versions of signal space and source space data. Feature extraction significantly improved performance across all domains. The highest classification accuracy of 0.98 was achieved under the feature-based, specifically Katz FD (F2) signal space condition. Among source space analyses, the 1-parameter projection model with the statistical feature set (F1) performed best (0.84) and had an accuracy of 0.68 in F2, while the 3-parameter model reached a maximum of 0.75 with F2 features. These results show that even with a fixed dipole location and single-source waveform, classification is possible, and that increasing model complexity slightly improves performance.

Future work should explore models involving multiple dipole locations or multi-node patched waveform representations to enrich the spatial and temporal information available for classification. The finding supports the integration of such techniques into future clinical tools aimed at automating IED detection and improving diagnostic workflows in epilepsy.

Contents

List of tables

List of figures

List of Symbols

Symbol	Description
x_i	EEG signal amplitude at time point i
N	Total number of time points in an epoch
$\bar{x}$	Mean amplitude of the EEG signal within an epoch
σ	Standard deviation of the EEG signal
S	Skewness of the signal distribution
K	Kurtosis of the signal distribution
$L_k(m)$	Length of the time series at scale k, starting from point m (Higuchi FD)
L_k	Average curve length for scale k (Higuchi FD)
D_H	Higuchi Fractal Dimension (F5)
L	Total length of the signal in Katz FD (F6)
d	Maximum distance between the first point and any other point in the signal (Katz FD)
D_K	Katz Fractal Dimension (F7)
λ	Lyapunov Exponent (F8)
$\mathbf{w}_k$	Weight vector at iteration k in SCG training
$\mathbf{E}'(\mathbf{w})$	Gradient of the total error with respect to $\mathbf{w}$
k	Iteration index
$\mathbf{p}_k$	Conjugate search direction vector at iteration k
λ_k	Damping parameter at iteration k (ensures positive definiteness of Hessian approximation)
σ_k	Scaling parameter at iteration k (step size for finite-difference approximation)
$\mathbf{s}_k$	Approximation of the Hessian–vector product at iteration k

Table 1

List of mathematical symbols used in the Methods section.

List of Abbreviations

Abbreviation	**Definition**
EEG	Electroencephalography
sEEG	Stereoelectroencephalography
IED	Interictal Epileptiform Discharge
MRI	Magnetic Resonance Imaging
BEM	Boundary Element Model
ANN	Artificial Neural Network
SCG	Scaled Conjugate Gradient
PSD	Power Spectral Density
FFT	Fast Fourier Transform
HFD	Higuchi Fractal Dimension
KFD	Katz Fractal Dimension
GoF	Goodness of Fit
EP1, EP2, EP3	Epileptologist 1, 2, and 3 (Labeling Experts)
ORmarking	Epoch labeled as spike by *at least one* epileptologist
ANDmarking	Epoch labeled as spike by *all three* epileptologists

Table 2
List of abbreviations.

1 Introduction

1.1 Epilepsy: Clinical Background and Diagnosis

Epilepsy is a chronic neurological disorder that affects more than 50 million people worldwide, making it one of the most prevalent brain conditions (World Health Organization, 2022). It is characterized by a persistent predisposition to generate unprovoked, recurrent seizures due to abnormal or excessive neuronal activity (Fisher et al., 2014). These seizures may result in abrupt changes in behavior, sensation, awareness, or motor function. A key mechanism underlying many epileptic seizures is hypersynchrony, in which large groups of neurons fire simultaneously in an uncontrolled manner (Milligan, 2021).

Approximately 70% of individuals with epilepsy can achieve seizure freedom through appropriate diagnosis and treatment (Milligan, 2021; World Health Organization, 2022). However, epilepsy also has broader implications, often affecting cognitive, psychological, and social functioning (Sarmast et al., 2020).

The classification of seizures begins with identifying their onset. Seizures are broadly categorized as either focal or generalized. Focal seizures, also referred to as partial seizures, originate within a specific region or lobe of the brain. In contrast, generalized seizures affect both hemispheres simultaneously and may not arise from a clearly defined focus (Hussein et al., 2018; P.A. & Desai, 2023; Sarmast et al., 2020). Proper classification is essential for accurate diagnosis and treatment planning (Milligan, 2021).

The initial evaluation of a patient following a first seizure should be performed by a physician, and referral to an epilepsy specialist is recommended if epilepsy is suspected (Nunes et al., 2012). A timely diagnosis allows for the initiation of personalized treatment strategies. Electroencephalography (EEG) plays a central role in epilepsy diagnosis by identifying abnormal brain activity and distinguishing focal from generalized seizure types. In clinical practice, EEG is often used in conjunction with neuroimaging techniques such as magnetic resonance imaging (MRI) to detect structural abnormalities in the brain (Milligan, 2021).

The first line of treatment typically involves antiepileptic drugs (AEDs), which are selected based on seizure type and patient response. Narrow-spectrum AEDs may be effective for focal seizures but are less so for generalized types, whereas broad-spectrum AEDs can be used across multiple seizure types. For patients with drug-resistant epilepsy, which is defined as failure to respond to two or more AEDs, surgical interventions such as temporal lobectomy, MRI-guided laser ablation, or

implantation of neurostimulation devices may be considered (Milligan, 2021). In addition, dietary therapies like the ketogenic diet have shown promise in seizure reduction for certain patients (Shaaban et al., 2023). Ultimately, the goal of epilepsy treatment is to achieve seizure control while minimizing side effects and enhancing the quality of life.

1.2 Electroencephalography (EEG) in Epilepsy

Electroencephalography (EEG) is a non-invasive neurophysiological technique that is widely used in the diagnosis and classification of epilepsy. By detecting the electrical activity generated by synchronized neuronal firing in the cerebral cortex, EEG provides a real-time representation of brain wave patterns through electrodes placed on the scalp (St. Louis et al., 2016). Its ability to capture abnormal brain activity during and between seizures makes it a cornerstone in epilepsy diagnostics.

EEG signals primarily reflect postsynaptic potentials from cortical neurons. Electrodes are placed at standardized scalp locations according to systems such as the international 10–10 system, ensuring consistent spatial coverage of brain regions including the frontal, temporal, parietal, and occipital lobes (Mecarelli, 2019).

Epileptiform activity can be broadly categorized as ictal, occurring during a seizure, and interictal, occurring between seizures (Rosenow & Lüders, 2001). Ictal EEG patterns are used to localize the seizure onset zone, the brain area where seizures originate, whereas interictal epileptiform discharges (IEDs), such as spikes, sharp waves and spike-wave complexes, are used to localize the irritative zone, the region generating abnormal discharges outside seizure periods. Although traditionally considered distinct, recent studies have shown that IEDs and seizures share similar probability distributions, suggesting they are not wholly independent processes(Karoly et al., 2016). Importantly, complete resection of regions generating IEDs has been linked to significantly improved long-term postoperative seizure outcomes, even at 5-10 years of follow-up (Rampp et al., 2019).

These characteristic patterns allow clinicians to differentiate epileptic from non-epileptic events and help localize the brain regions responsible for seizure onset (Noachtar & Rémi, 2009). Recent advances in signal processing and neuroimaging have expanded the capabilities of traditional EEG. Source imaging techniques, including Minimum Norm Estimation (MNE) and Local Auto-Regressive Average (LAURA), enable the transformation of scalp-level recordings into 3D cortical activity maps. These methods enhance the localization of epileptogenic zones, particularly when combined with high-density EEG, which offers improved spatial resolution and classification accuracy (Michel et al., 2004).

Epileptic seizures are typically classified as either generalized or focal. Generalized seizures, such as absence or myoclonic seizures, are marked by synchronous bilateral spike-and-wave discharges, often observed at 3 Hz in absence epilepsy. In contrast, focal seizures originate in specific brain regions, such as the anterior temporal lobe, and are often associated with localized interictal discharges. For example, mesial temporal lobe epilepsy commonly presents with temporal spikes and ictal rhythmic discharges that are restricted to the epileptogenic zone (Smith, 2005).

Despite its strengths, scalp EEG has several limitations. It may fail to detect deep or infrequent epileptiform activity, especially during short recording periods. Additionally, its spatial resolution is limited, making it difficult to localize small or deep-seated foci accurately (Smith, 2005). However, when combined with structural imaging such as MRI or invasive intracranial EEG, conventional EEG remains an essential component of a comprehensive diagnostic framework in epilepsy care.

1.3 Interictal Epileptiform Discharges (IEDs)

Misdiagnosis of epilepsy remains a significant clinical concern, with studies indicating that 20% to 30% of patients referred to epilepsy centers are initially misdiagnosed (Benbadis, 2009). A key element in achieving accurate diagnosis is the detection of interictal epileptiform discharges (IEDs) on EEG recordings. These paroxysmal events occur between seizures and are typically characterized by transient abnormalities such as sharp, high-amplitude peaks (spikes) and disruptions in the normal rhythm of brain activity (de Moraes & Callegari, 2014).

According to the International Federation of Societies for Electroencephalography and Clinical Neurophysiology (IFSECN), epileptiform patterns are defined as:

> *"Epileptiform patterns (epileptiform discharge or activity): transients distinguishable from background activity, with a characteristic spiky morphology, typically, but not exclusively or invariably, found in interictal EEGs of people with epilepsy."* (Noachtar et al., 1999)

IEDs play a critical role for clinical decision-making by aiding in the localization, classification and identification of epileptic foci. Their morphological characteristics serve as diagnostic markers for different epilepsy types and contribute to treatment planning (Ramakrishnan et al., 2025).

Interictal discharges can be morphologically categorized into several types, including spikes, sharp waves, spike-and-wave complexes, polyspikes, and polyspike-and-slow-wave complexes. The IFSECN provides the following definitions (Noachtar et al., 1999):

- **Spike:** A transient with a pointed peak and a duration between 20 and 70 milliseconds.
- **Sharp wave:** Similar to a spike but with a longer duration of 70 to 200 milliseconds.
- **Slow wave:** A waveform lasting longer than typical alpha rhythms, i.e., over 125 milliseconds.
- **Spike-and-slow-wave complex:** A spike followed immediately by a slow wave.
- **Multiple spike complex:** A sequence of two or more spikes occurring in rapid succession.
- **Polyspike-and-slow-wave complex:** Two or more spikes followed by one or more slow waves.

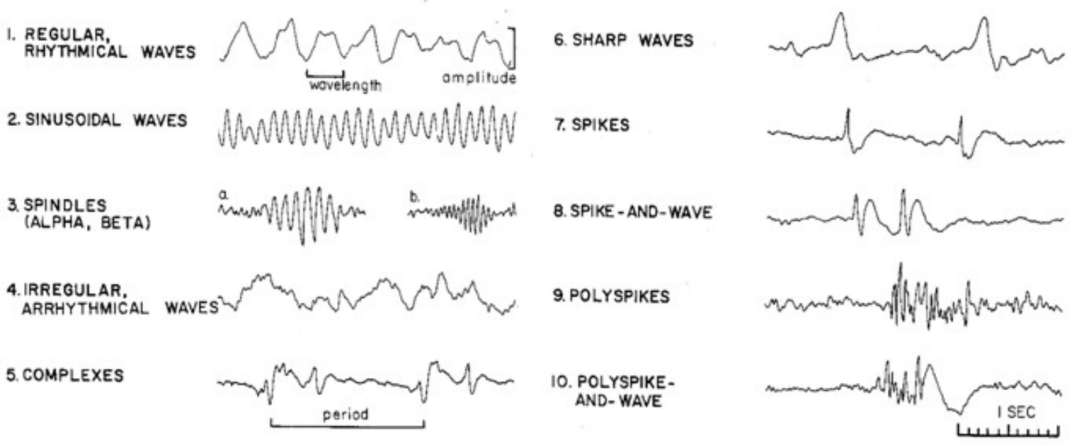

Figure 1
Examples of EEG waveforms and spike morphologies. Patterns 1-5 represent normal background rhythms. Patterns 6-10 are characteristic epileptiform morphologies typically observed in interictal EEG.

The morphological analysis of IEDs plays a central role in improving diagnostic accuracy and guiding clinical decisions. A recent clinical study introduced the Bergen Epileptiform Morphology Score (BEMS), which quantifies the morphology of sharp transients in EEG data. BEMS ranges from 0 to 86, with higher scores indicating morphologies more typical of epileptiform discharges (Aanestad et al.,

2023). The score is derived from a weighted combination of visually interpretable morphological features, including spike slope, spike amplitude, similarity of the spike to background activity, slow after-wave area, and patient age (as IED morphology is age-dependent). The specific upper limit of 86 results from the summation of these weighted feature contributions in the original scoring system, as defined in prior methodological work by Aanestad et al., 2023

1.4 Spike Detection Techniques

Spike detection refers to the identification of transient, high-amplitude waveforms in EEG recordings, typically with durations between 20 and 70 milliseconds for spikes and 70 to 200 milliseconds for sharp waves (Aminoff, 2012). Accurate detection of these events is essential for the diagnosis and classification of epilepsy, as they represent key indicators of interictal epileptiform activity.

However, several challenges complicate manual spike detection. These include a low signal-to-noise ratio, variability in spike morphology across patients and recording sessions, and the inherent subjectivity involved in visual annotation by clinicians (Holleman et al., 2011). Such limitations can lead to inconsistent interpretations and an increased risk of misdiagnosis.

To address these issues, a wide range of automated spike detection algorithms have been proposed over the past few decades. These methods leverage signal processing and pattern recognition techniques to identify spikes within noisy EEG data and, in some cases, classify them based on spatial or morphological characteristics. Automated approaches have shown promise in reducing false positives, improving inter-rater agreement, and streamlining clinical workflows (Kim & Kim, 2000).

With the advancement of machine learning, particularly neural networks, recent research has focused on developing data-driven models capable of learning discriminative features directly from EEG signals (Ma et al., 2024). These models aim to improve the accuracy and generalizability of spike detection, reducing the need for extensive manual preprocessing or expert annotation (Kumar & Upadhyay, 2025). This trend reflects a broader shift toward intelligent systems in neurodiagnostics and forms the foundation for the current study, which evaluates the effectiveness of artificial neural networks (ANNs) in detecting IEDs from both signal-space and source-space EEG data.

1.5 Signal Space vs. Source Space Analysis

In EEG research, data analysis can be approached from two perspectives: signal space and source space.

Signal Space Analysis involves examining the electrical activity recorded directly from scalp electrodes. This method is straightforward and does not require complex computational models. However, it is limited by the effects of volume conduction, in which electrical signals from different brain regions mix as they pass through the skull and scalp. This mixing can lead to reduced spatial resolution and the introduction of spurious sensor-level connections. Studies have shown that volume conduction can cause misleading interpretations of connectivity when analyses are confined to the sensor level (van de Steen et al., 2016).

Source Space Analysis aims to estimate the locations and activities of neural generators within the brain by applying inverse modeling techniques to the scalp-recorded EEG data. This approach mitigates some limitations of signal-space analysis by providing a more accurate representation of the underlying neural sources. Source waveforms estimated through such analyses are generally assumed to have a higher signal-to-noise ratio (SNR) than spontaneous signal-space data, which facilitates the identification and localization of interictal spikes (Kirsch et al., 2006). By reconstructing brain activity in the source space, researchers can achieve improved spatial resolution and more precise localization of neural events. For instance, source-space functional connectivity analysis has been utilized to examine interactions between different cortical regions, offering insights that are less susceptible to the confounding effects of volume conduction (Barzegaran & Knyazeva, 2017).

1.6 Study Objectives and Contributions

In this thesis, we focus on machine learning spike marking in both source space and signal space. The pipeline consists of three primary stages: data preparation, source analysis, and model training. Each stage contributes to enhancing the reliability and accuracy of interictal spike detection using neural networks.

Preprocessing ensures data quality, source analysis allows spatial localization of neural generators and yields source waveforms with potential improved signal-to-noise ratio (SNR), and the machine learning stage enables automated classification. As illustrated in Figure 2, the data preparation step includes filtering and epoching EEG signals, followed by spike annotation. Source analysis incorporates MRI-based head modeling and moving dipole fit for source localization, continued with source waveform projection. Finally, both signal-space and source-space data are used to

train artificial neural networks (ANN) for classification.

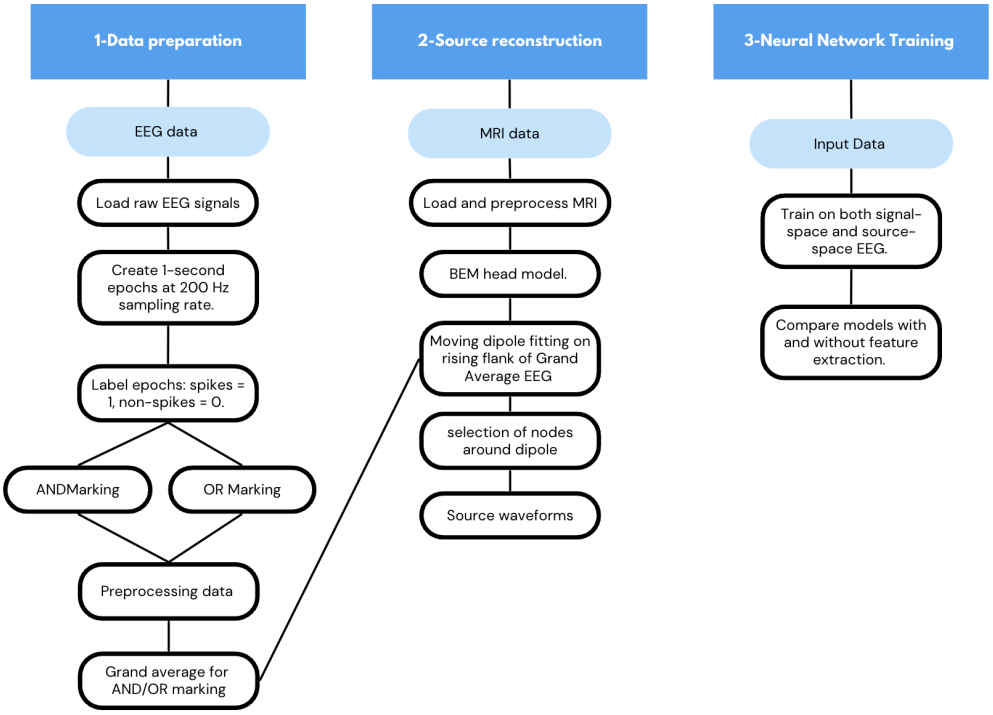

Figure 2
Spike detection pipeline comprising three stages: data preparation, MRI-based source reconstruction (allowing spatial localization and potentially improved SNR), and neural network training using both signal-space and source-space EEG.

2 Methods

2.1 Data collection

EEG data were obtained from a single patient: a 26-year-old female diagnosed with refractory focal epilepsy originating in the left frontal lobe, near Broca's area. The patient had experienced epileptic seizures since the age of 14 and received treatment at Münster University Hospital between 2018 and 2023.

Episodes of impaired thinking and an inability to communicate or follow conversation, without motor symptoms or impaired awareness, were characteristic of seizure semiology. The frequency of seizures ranged from once a week to as often as four times a day. No seizures involving loss of awareness, motor involvement, or secondary generalization were reported. Despite treatment with multiple anti-seizure

medications, the patient did not achieve seizure freedom. Since the clinical criteria for pharmacoresistance were met, a first presurgical evaluation for potential resective epilepsy surgery was performed in 2018 (Antonakakis et al., 2024). However, the initial invasive EEG study was inconclusive in localizing the seizure onset zone.

A total of 22 hours of EEG data were acquired and separated into 22 one-hour sessions. The recordings were obtained using a clinical EEG system with 19 electrodes, corresponding to a subset of the international 10-20 system (Hinrichs et al., 2020). All EEG data were recorded at a sampling frequency of 200 Hz.

The study was conducted in accordance with the Declaration of Helsinki and was approved by the Institutional Ethics Review Board (Ethik-Kommission der Ärztekammer Westfalen-Lippe und der Westfälischen Wilhelms-Universität Münster, approval date: May 25, 2021, Ref. No. 2021-290-f-S). The patient provided written informed consent for the use of her anonymized data for scientific research and publication. In this thesis, no identifiable patient information is presented to preserve complete anonymity.

2.2 Tools and Software

All computational work in this thesis was conducted using MATLAB R2024b, which served as the primary environment for data processing, EEG analysis, model development, and performance evaluation. Several MATLAB toolboxes were used to support different aspects of the workflow. The FieldTrip Toolbox, an open-source package designed for MEG/EEG data analysis (Oostenveld et al., 2011), was employed for EEG data import, temporal alignment of epochs, grand-averaging of waveforms, and dipole fitting. The Deep Learning Toolbox was used for the implementation, training, and evaluation of Artificial Neural Networks, including binary classification tasks (The MathWorks, 2023a). The Signal Processing Toolbox facilitated digital filtering as well as spectral and temporal analysis during preprocessing, while the Statistics and Machine Learning Toolbox was used to compute performance metrics such as confusion matrices, precision, and recall (The MathWorks, 2023b, 2023c).

Several other toolboxes (e.g., Bioinformatics, Predictive Maintenance, and System Identification Toolboxes) were available in the MATLAB environment but not directly used in the analysis. These are noted for completeness.

To supplement the capabilities of these toolboxes, a set of custom MATLAB scripts was developed to perform processing steps not natively supported by FieldTrip, such as data structuring, class balancing, and automated performance metric computation. These scripts, together with full analysis pipeline, are openly available

for reproducibility and further research at through a GitHub repository.[1]

2.3 EEG Preprocessing

EEG preprocessing was a crucial step in ensuring signal quality and preparing data for spike detection. Initial preprocessing involved exclusion of non-EEG channels, retaining only the 19 relevant clinically relevant electrodes based on the international 10-20 system (Hinrichs et al., 2020). The spatial layout of these electrodes is shown in Figure 3.

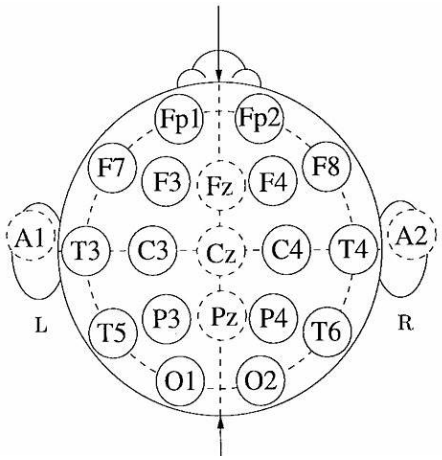

Figure 3
The 19-channel EEG electrode layout based on the international 10–20 system used in this study.

To mitigate artifacts and enhance signal clarity, a bandpass filter (0.5–40 Hz) was applied to continuous EEG data to remove low-frequency drifts and high-frequency noise. Although the low-pass cutoff at 40 Hz attenuates most of the 50 Hz power-line interface, a notch filter at 50 Hz was additionally applied to ensure complete suppression of residual line noise and harmonics.

Following these steps, the preprocessed EEG recordings (22 hours in total) were divided into non-overlapping 1-second epochs. Given the sampling rate of 200 Hz, each epoch contained 200 samples, resulting in a total of 79,876 epochs for subsequent analysis.

The preprocessed and segmented EEG data were then utilized for the manual annotation of interictal epileptiform discharges (IEDs) by independent epileptologists. These annotations served as the basis for defining spike-containing (label = 1) or non-spike (label = 0) epochs. A detailed description of the labeling process and the resulting dataset organization is provided in Section 2.4.

[1] https://github.com/cafaroval/ML_spike_detection

2.4 Labeling Process

Interictal Epileptiform Discharges (IEDs) were manually annotated in the continuous EEG recordings by three independent epileptologists (EP1, EP2 and EP3). For annotation purposes, each of the 22 one-hour EEG recordings was segmented into non-overlapping 1-second epochs, resulting in a total of 79,876 epochs. Each epoch comprised 200 samples with a dimensionality of 19 channels x 200 time points.

Each epileptologist independently labeled epochs that they judged to contain IEDs. Based on this process, EP1 identified 2890 spike epochs, EP2 identified 1646, and EP3 identified 10279. Epochs labeled as containing IEDs were categorized as spike epochs, while all remaining epochs were labeled as non-spike. Table 3 summarizes the number of spike and non-spike epochs identified by each epileptologist. As shown, there is considerable variability among reviewers in the number of IEDs detected, which reflects the inherent subjectivity in visual EEG interpretation. Additionally, across all epileptologists, non-spike epochs outnumber spike epochs, highlighting a substantial class imbalance in the dataset.

Epileptologist	**Epochs Containing IED**	**Epochs Without IED**
EP1	2,890	76,986
EP2	1,646	78,230
EP3	10,279	69,597

Table 3
Number of epochs labeled as containing or not containing IEDs by each epileptologist.

Due to this strong class imbalance between spike and non-spike epochs, specific steps were taken to address this issue during model development to ensure fair and robust classification performance. This was handled during data preparation for the ANN model, as described in Section 2.6.

To reduce the subjectivity inherent in individual expert annotations and to explore the impact of labeling strategy on model performance, the labeled data were grouped into two strategies:

- **ANDmarking**: Includes only epochs marked as containing IEDs by all three epileptologists. This conservative labeling strategy ensures higher certainty that labeled spikes reflect true epileptiform activity.
- **ORmarking**: Includes epochs marked by at least one epileptologist, which therefore includes all AND-marked epochs. This approach increases sensitivity

to potentially subtle or ambiguous spike events, though it may also increase more label uncertainty.

These two labeling strategies are directly used in generating model inputs for classification, beginning with the source space data derivation in the next subsection.

2.5 Source Localization

This section describes the process of transforming scalp-recorded EEG data into a source-level representation. This involves constructing a realistic head model, computing the forward model (lead field matrix), averaging spike epochs and projecting them into the estimated source space, with the goal of producing source waveforms with a high signal-to-noise ratio (SNR) at interictal epileptiform discharges (IEDs).

2.5.1 Averaging spike epochs

To characterize the temporal profile of IEDs for source localization, grand-average spike waveforms were computed separately for epochs identified by the AND marking strategy and OR marking strategy. Averaging across N spike events should theoretically increase the signal-to-noise ratio (SNR) by a factor of $\sqrt{N}$, thereby revealing the consistent underlying electrophysiological activity while suppressing random noise.

For this alignment, electrographic seizure patterns were predominantly recorded in the left frontal area, often presenting with a maximal negativity at the F3 electrode. Therefore, individual spike epochs were temporally aligned to the negative peak of the F3 channel, which consistently exhibited the highest negativity compared to other channels. Non-spike epochs, by definition lacking a consistent physiological peak of alignment, were not subject to this peak-based temporal alignment. Instead, they were collected as 1-second segments, aligned only to their epoch boundaries.

For subsequent dipole fitting, the grand average spike waveforms were carefully examined to identify a stable and representative period representing the rising phase of the IED. The time window of [-20 ms, -5 ms] relative to the aligned F3 negative peak was selected for dipole fitting. This specific window, visually marked by dashed vertical lines in Figures 4 and 5, was chosen for the following reasons:

- **Physiological Relevance:** The rising flank of an IED is generally considered to represent the initial, highly synchronized depolarization of a neuronal population and is the primary generator of the characteristic scalp-recorded spike potential. Many studies have suggested reconstructing sources at the middle

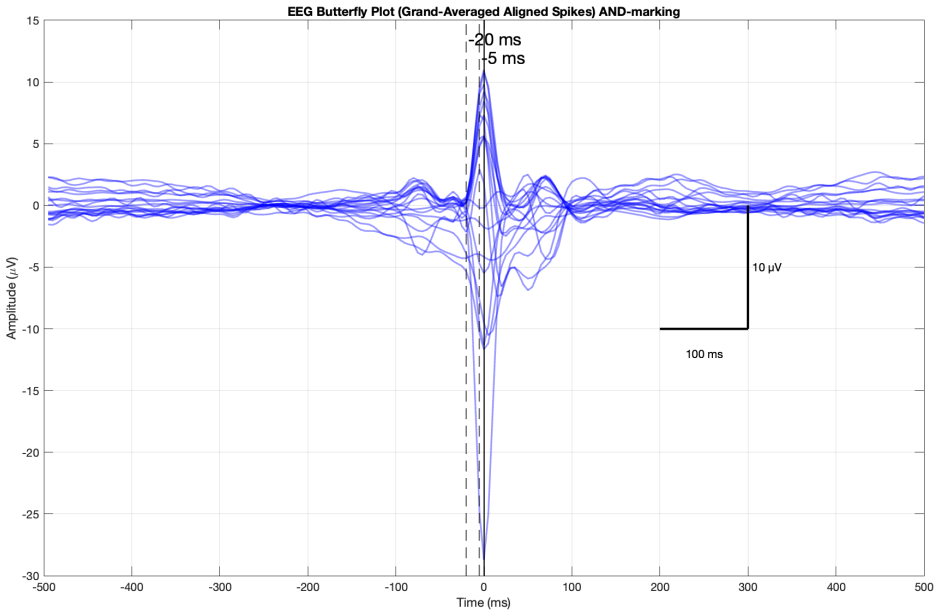

Figure 4

Grand average of IED epochs identified by the conservative AND-marking strategy. Epochs are aligned to the negative peak of the F3 channel (at 0 ms). The dashed vertical lines indicate the [-20 ms, -5 ms] time window used for dipole fitting.

of the rising flank rather than at the spike peak, as the latter can be affected by propagation and yield misleading localizations(Aydin et al., 2015, 2017; Lantz et al., 2003). This early rising phase tends to provide a more stable and physiologically meaningful estimate of the source localization compared to analyzing the sharper, more variable peak or complex falling phase (Forjaco Jorge, 2016; Myers et al., 2020). Propagation effects have been clearly demonstrated, including in Antonakakis et al., 2024, where source analysis localized activity deeply within the sulcus at spike onset but to the gyral crown at spike peak. For the present work, projecting the data to a source space that encompasses both regions or to a location approximately midway between these extrema was deemed a reasonable approach.

- **Signal Stability:** The interval from -20 ms to -5 ms typically precedes the sharpest and most variable part of the spike peak, which can be susceptible to transient artifacts or minor temporal jitters across trials. By selecting this segment, we aimed to capture the more consistent, underlying build-up of the epileptic discharge, enhancing the robustness of the dipole fit (Vulliemoz,

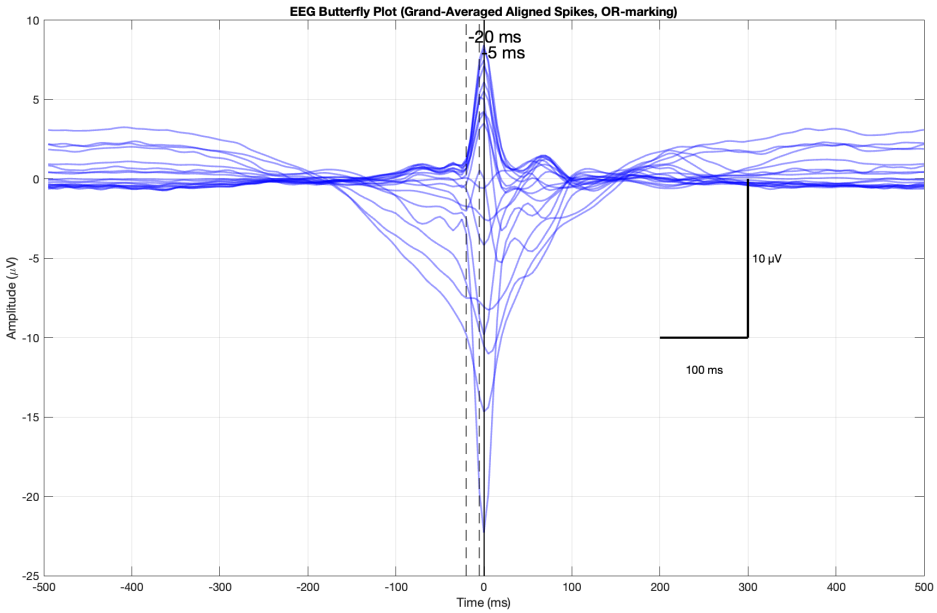

Figure 5

Grand average of IED epochs identified by the more sensitive OR-marking strategy. Epochs are aligned to the negative peak of the F3 channel (at 0 ms). The dashed vertical lines indicate the [-20 ms, -5 ms] time window used for dipole fitting.

2012).

- **Consistency with Alignment:** As the individual spike epochs were aligned based on the F3 peak, selecting a window relative to this established reference point ensures temporal consistency for the dipole estimation across all averaged spikes(Ramantani, 2018).

2.5.2 Head Model and Lead Field Construction

Accurate localization of the EEG source requires a realistic head model and a well-defined lead field matrix. To understand this, it's important first to grasp fundamental concepts of forward modeling and inverse modeling.

As described in Figure 6, the forward problem in EEG is the process of computing the scalp potentials generated by known neural current sources (electrical currents) embedded within the brain, using a comprehensive model of how electrical current conducts through the head (i.e., volume conduction through body tissues) (Brette & Destexhe, 2012; Doschoris & Kariotou, 2017; Wolters & Munck, 2007). Solving the forward problem involves understanding the biophysics of current flow through

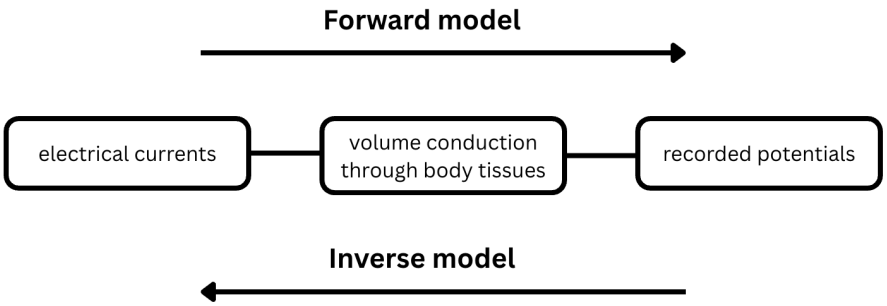

Figure 6
Conceptual illustration of the Forward and Inverse Problems in EEG.

different tissue types (brain, cerebrospinal fluid, skull, and scalp). Methods such as the Boundary Element Method (BEM), Finite Element Method (FEM) and Finite Difference Method (FDM) are routinely employed to compute the electric potential distribution on the scalp (Gramfort et al., 2010; Höltershinken et al., 2025). The output of the forward model, the lead field matrix, mathematically describes the contribution of each possible neural source location to the potential at each scalp electrode (Doschoris & Kariotou, 2017).

Furthermore, the inverse problem in EEG aims to determine the location, orientation, and strength of neural sources (electrical currents) within the brain based on the non-invasively measured electrical potentials on the scalp (recorded potentials). This is a significantly more challenging problem than the forward problem because it is inherently ill-posed. This means that multiple different source configurations within the brain could theoretically produce the same set of measured scalp potentials (Brette & Destexhe, 2012; Jatoi et al., 2014). Therefore, inverse modeling requires the application of additional constraints, assumptions, and computational techniques to arrive at a physiologically plausible and unique solution (Bekhti, 2018; Brette & Destexhe, 2012).

This subsection outlines the comprehensive anatomical and electrophysiological data processing pipeline implemented using the FieldTrip toolbox, designed to prepare the data for source reconstruction by accurately addressing the forward problem, which is a crucial prerequisite for subsequent inverse modeling.

The workflow began with the import of a T1-weighted structural MRI scan. The MRI volume was interactively realigned to the CTF coordinate system using fiducial landmarks (nasion, left preauricular point and right preauricular point) to ensure

anatomical accuracy. The realigned volume was then resliced to obtain isotropic voxel dimensions and standardized orientation.

Tissue segmentation was performed to isolate brain, skull and scalp compartments. These segmented volumes were used to construct a realistically shaped, three-compartment (skin, skull, brain) boundary element model (BEM), in which each tissue layer was represented as a triangular mesh on the surface. The resulting BEM, computed using the OpenMEEG software package Gramfort et al., 2010, served as the volume conduction model for subsequent EEG source modeling (Fuchs et al., 2002; Kybic et al., 2005).

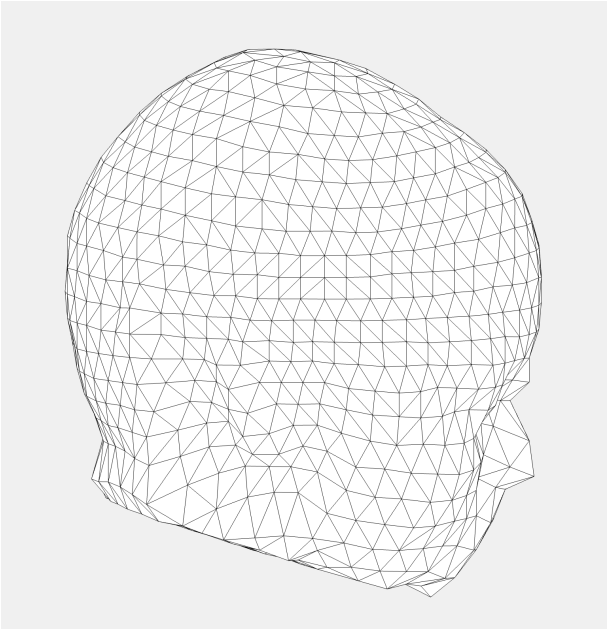

Figure 7
Triangular mesh on the surface.

Electrode positions were extracted from a standard 10-20 system file, and 19 relevant channels were selected and interactively aligned to the MRI-derived scalp surface. This ensured accurate spatial correspondence between electrodes and a participant's unique head anatomy.

A 3D source grid with 3 mm resolution was generated within the brain volume, and all components were standardized to millimeter units to ensure consistency. The lead field matrix was then computed using the head model (BEM) EEG forward modeling as implemented in OpenMEEG and integrated in FieldTrip Gramfort et al., 2010; Kybic et al., 2005. This computation enables the forward projection of neural sources to scalp potentials (Brette & Destexhe, 2012). The setup was visually inspected for anatomical and spatial consistency, ensuring the validity of the forward model for subsequent source reconstruction.

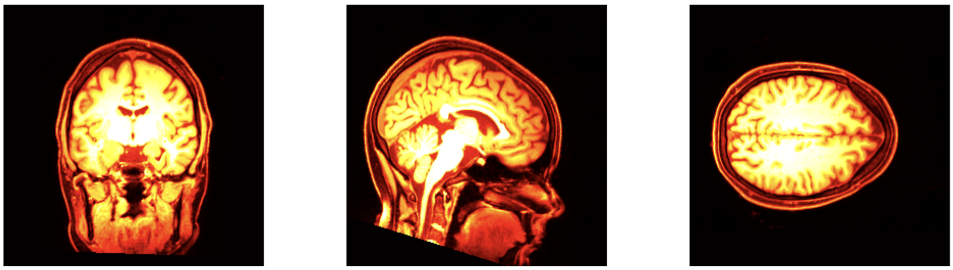

Figure 8
Orthogonal MRI slices showing coronal (left), sagittal (middle), and axial (right) planes at voxel coordinates. The image reflects the realigned and resliced structural T1-weighted MRI volume used for head model construction.

2.5.3 Dipole fitting

Following the construction of the head model and lead field, a single equivalent current dipole (ECD) was estimated to represent the neural source of the grand average spike waveforms. This process was performed separately for the AND-marking and OR-marking strategies.

Specifically, the dipole fitting was conducted on the rising flank of the averaged spike signal within a carefully selected time window of [-20 ms, -5 ms] relative to the aligned F3 negative peak. This window was chosen for the physiological and signal stability reasons detailed in Section 2.5.1. The dipole estimation was performed using the FieldTrip toolbox, leveraging the previously constructed realistic BEM head model and computed lead field matrix to accurately model the forward projection of neural sources to scalp electrodes. A single dipole model was employed, and the fitting algorithm was set to a 'moving' model, allowing the dipole to vary its position and orientation within the specified latency window.

From the results of the dipole fitting, the position and orientation of the best-fitting dipole within the selected time window were extracted for both the AND-marked and OR-marked grand averages. The peak Goodness of Fit (GoF) for the AND marked grand average was calculated as 99.29% , and for the OR marked grand average as 99.04% i.e., a very high GoF showing that the model explains the data well. While these values are higher than those reported in Antonakakis et al., 2024 for EEG rising-flank fits (e.g., 91%), the difference may be explained by methodological differences.

To assess whether a fixed dipole orientation assumption was valid, the GoF was evaluated at multiple time points across the rising flank using 3-parameter projection. As shown in Figure 9, GoF exhibited substantial temporal fluctuations,

suggesting that the source orientation changes over the course of the spike. This indicates that projecting the data onto a single fixed orientation could distort the waveforms, whereas retaining the full three-component (3D) source waveform would preserve physiologically relevant orientation dynamics.

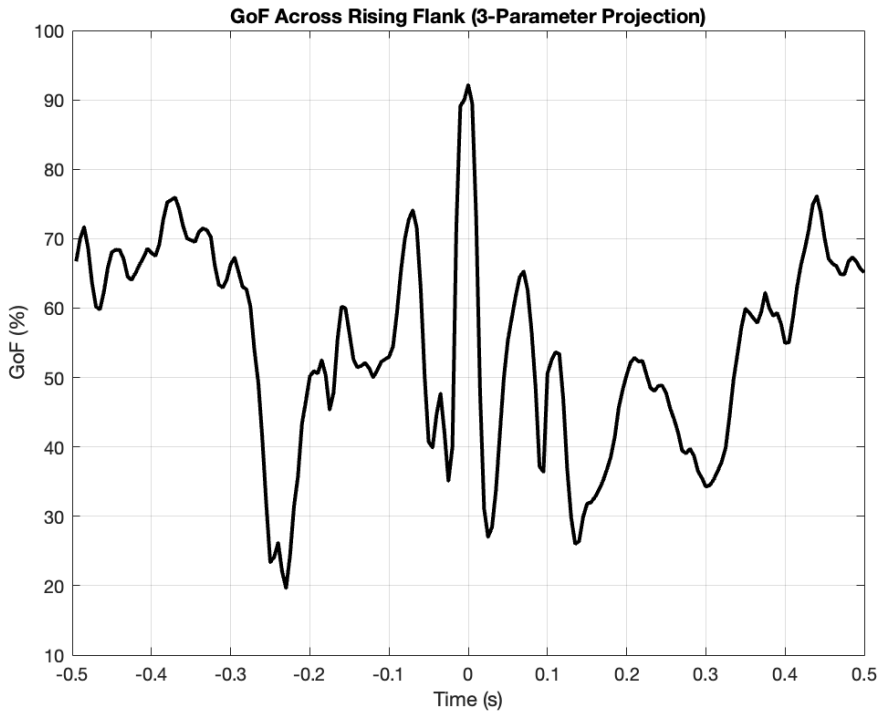

Figure 9

Goodness of Fit over time during the rising flank of the averaged IED, computed using a 3-parameter dipole model. Large fluctuations in GoF indicate changes in the scalp potential pattern over time, suggesting rotation of the underlying source orientation. This supports the use of §D projection to preserve waveform fidelity.

The fitted dipoles for both AND-marked and OR-marked grand averages are shown in Figure 10. These dipoles were consistently localized to the left frontal lobe, in close proximity to the F3 EEG electrode, and anatomically consistent with the seizure onset zone as detected by sEEG, which was guided by combined EEG/MEG source analysis in Antonakakis et al., 2024.

2.5.4 Selection of Cortical Source Nodes

After estimating the dipole for the grand average spike signal, the next step involved selecting a set of source nodes for projection. The aim was both to focus

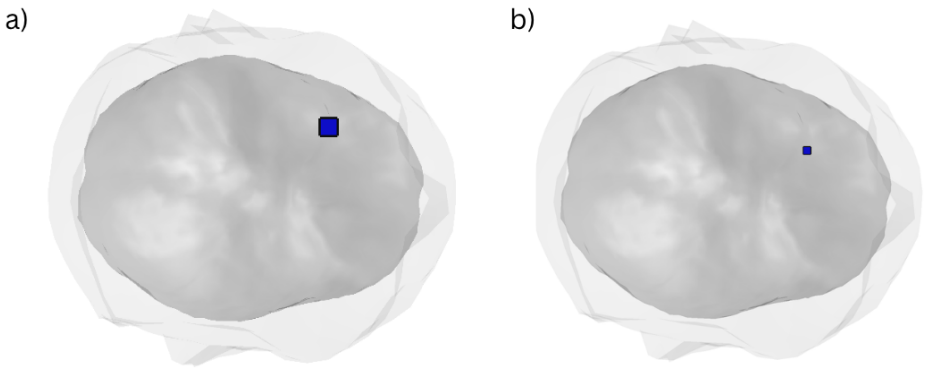

Figure 10
Estimated equivalent current dipoles (blue) representing the source of the grand average IEDs at -5 ms relative to the aligned F3 negative peak, corresponding to the last time point of the moving dipole fit window. a) Fitted dipole for the global average over AND-marking spikes. b) Fitted dipole for the global average over OR-marking spikes. In both panels, the dipoles are shown within a transparent head model, viewed from a superior (top) perspective. The spatial separation between the two source locations is approximately 11.35 mm, indicating a moderate difference between the two marking strategies.

the analysis on the most physiologically relevant brain regions surrounding the estimated IED generator and to reduce the dimensionality of the inverse problem for subsequent machine learning tasks.

The selection was carried out in two stages. First, an anatomically constrained bounding box was defined within the left frontal lobe of the cortical surface. The bounding box coordinates were chosen manually by inspecting the MRI source grid to ensure coverage of the presumed source region. The process involved:

1. Identifying all valid source grid points that were marked as 'inside' the brain volume in the source model.

2. Defining specific minimum and maximum CTF coordinates along the anterior-posterior (X), left-right (Y) and inferior-superior (Z) axes to encompass the desired region.

3. Including only those source grid points that fell precisely within these defined

coordinate ranges and were confirmed to be inside the brain volume.

All valid grid points located inside the brain volume and within these boundaries were included as an initial candidate set of nodes. This stage was used in the one-parameter projection analysis, where the orientation was fixed and a larger number of nodes were retained.

In the second stage, used for the three-parameter projection analysis, the candidate pool was refined to a compact patch of nodes directly surrounding the fitted dipole. Specifically, the ten closest nodes to the dipole position were selected based on Euclidean distance in three-dimensional space. This step ensured that the final node set captured the immediate cortical neighborhood of the estimated generator while maintaining a manageable number of nodes for projection.

Together, these two approaches provided complementary ways of defining the cortical source space, a broader anatomically guided set for the 1-parameter projection, and a more focused, spatially specific patch for the three-parameter projection.

2.5.5 Source Waveform projection

Following dipole fitting and selection of cortical source nodes for both AND and OR marking strategies, the next critical step involved projecting the scalp-level EEG data into the source space to produce source waveforms. This methodology first determined the source location through dipole fitting and then utilized these predetermined locations to spatially filter the scalp potentials. This process provided an estimate of neural activity at targeted brain regions. This approach was applied for both grand average and for individual trial data, covering both spike and non-spike events for both marking strategies.

The source projection was formulated as a least-squares fitting problem between the measured EEG and the forward-modeled lead field at the chosen source location. For each selected node, the lead field matrix $L \in \mathbb{R}^{M\times 3}$ (with M sensors and three orthogonal source orientations) was used to solve:

$$\min_{J} \ \|\Phi - LJ\|_2 \tag{1}$$

where $\Phi \in \mathbb{R}^{M\times T}$ represents the EEG measurements over T time points, and $J \in \mathbb{R}^{3\times T}$ contains the source waveforms for the three orientations (x, y, z). The analytic solution is:

$$J = \left(L^\top L\right)^{-1} L^\top \Phi \tag{2}$$

Two cases can be distinguished:

1. **Fixed orientation (1D)**: The orientation vector is determined from the grand average dipole fit and applied to all time points, yielding a single waveform. This case assumes the EEG topography remains stable throughout the spike.

2. **Free orientation (3D)**: All three components of J are retained, allowing the estimated source orientation to vary over time. This is more flexible when the EEG pattern rotates during the spike, as may occur due to propagation or cortical folding.

In cases where the EEG topography over the spike is stable (no significant rotation), this model can be simplified to a single orientation, reducing J to $1 \times T$ and effectively yielding one source waveform. This is advantageous in focal epilepsy cases with a well-localized and fixed generator, as it reduces noise from unnecessary degrees of freedom.

Conversely, if the EEG pattern rotates during a spike retaining all three orientation components is necessary to compute the evolving spatial pattern. This projection framework therefore allows both scenarios to be implemented and compared, enabling quantification of their fit to the data over time.

For patch level projection, $K = 10$ cortical nodes were selected around the fitted dipole position for each strategy. Node selection was based on Euclidean distance from the fitted dipole coordinates within the anatomically defined cortical surface, ensuring that the chosen patch represented the spatial neighborhood of the estimated generator. For the patch, the lead field of the K nodes were concatenated into a joint matrix $L_{\text{patch}} \in \mathbb{R}^{M \times 3K}$, providing three degrees of freedom per node. The inverse problem was then solved using Tikhonov regularization to stabilize the solution, with the regularization parameter λ chosen automatically for each strategy using the L-curve criterion (maximum curvature point on the log-log residua-solution norm curve).

In the fixed orientation case, the chosen dipole orientation from the grand average was applied uniformly to all patch nodes, effectively creating a spatial filter that assumed all nodes shared the same temporal dynamics and source direction. In the free orientation case, each node's full three-component lead field was used to estimate J without constraining orientation, allowing each node to adapt to changing scalp topographies.

In the free orientation case, each node's three orthogonal source components were computed without imposing an orientation constraint, allowing the estimated source direction to vary over time. For visualization, $3K$ time series (three components for each of the K patch nodes) were combined by first computing the vector magnitude at each node and then averaging across the K nodes to yield a single representative

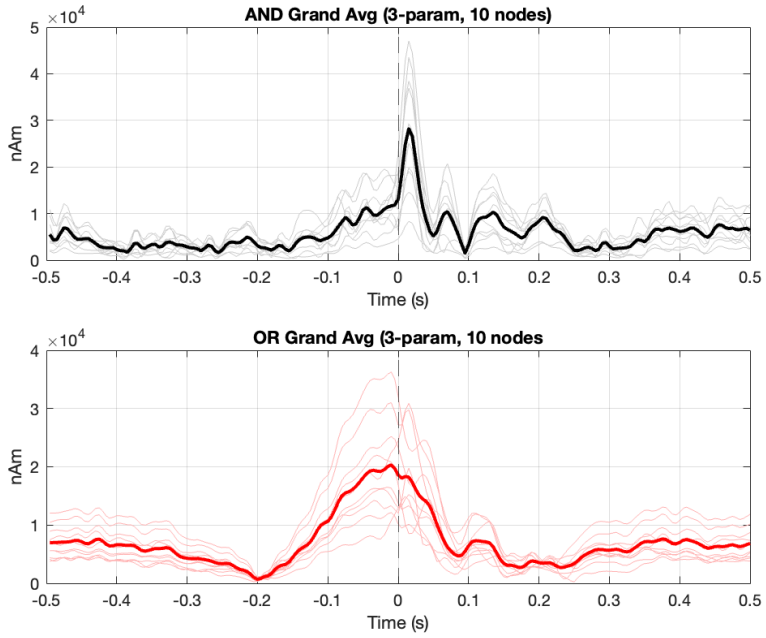

Figure 11

Patch-Level Source Waveforms for Grand Average IEDs. Vector magnitude of the 3-component (x,y,z) source estimates, averaged across the 10 closest cortical nodes to the fitted dipole location, expressed in nanoampere-meters (nAm) **a)** Grand-average source waveform for the AND-marked data. **b)** Grand-average source waveform for the OR-marked data.

waveform per marking strategy in Figure 11. This averaging step was performed only for plotting purposes. For trial-level analysis used in classification, no such averaging was applied.

2.6 Balancing the data

Following the projection of scalp-level EEG data into source space and having signal space data, a critical step involved balancing the number of spike and non-spike trials for each condition (AND/OR marking). This preprocessing is essential for subsequent machine learning tasks, as an imbalance in the number of samples between classes can lead to biased models that perform poorly on the minority class.

To address class imbalance, the spike and non-spike sets were randomly down-sampled to create balanced datasets containing equal numbers of examples from each class (Chawla et al., 2002). This ensured that the machine learning model would be trained on an equal representation of both event types, thereby preventing

a bias towards the more prevalent class and promoting robust model generalization.

After equalization, these balanced trial sets were combined into a single input dataset. Simultaneously, a corresponding binary target label array was created where 1 indicated a spike trial and 0 indicated a non-spike trial. This structured input and target labeling, which is fundamental for supervised machine learning, was then saved for the model training.

2.7 Artificial Neural Network (ANN)

Artificial Neural Networks (ANNs) are computational models designed to emulate the principles of the biological neural system, particularly those observed in the human brain (Abraham, 2005). In these models, the complex electrochemical processes of real neurons are abstracted into simplified mathematical units ("artificial neurons") that compute weighted sums of their inputs, apply nonlinear activation functions, and produce and outputs (Guilhoto, 2018).

An ANN typically consists of an input layer, which receives the raw data and one or more hidden layers, where intermediate transformations are performed. An output layer, which generates the final prediction (Agatonovic-Kustrin & Beresford, 2000). In the simplest case, there may be only a single hidden layer, whereas architectures with multiple stacked hidden layers fall into the category of deep neural networks (DNNs).

In this study, a feed-forward ANN with one hidden layer and a single output neuron was implemented for binary classification. This architecture was selected for its simplicity and effectiveness in modeling non-linear patterns in moderately sized data sets (Abdalla, 2011; Kavzoglu, 2001). The network processes input vectors through a hidden layer of 10 neurons with nonlinear activation functions, followed by one output neuron.

Prior to training, all input data underwent Z-score normalization (mean 0, standard deviation 1) to ensure consistent scaling across features, which aids in optimizing the training process (Çetin & Yıldız, 2022; Raju et al., 2020).

Training was conducted using the Scaled Conjugate Gradient (SCG) backpropagation algorithm, a second-order optimization technique that avoids line searches (Cetişli & Barkana, 2010). SCG was specifically developed to combine the advantages of both the Conjugate Gradient (CG) method and the Levenberg–Marquardt (LM) algorithm. It inherits the conjugate direction strategy from CG, which helps avoid redundant search paths. It incorporates a damping mechanism inspired by LM to stabilize the update process by adaptively adjusting the step size in regions of uncertain curvature. This makes SCG a robust and efficient choice for neural

network training, particularly for medium-scale problems.

In the SCG method, the search direction is updated using a finite-difference approximation to the Hessian-vector product. Let $\mathbf{E}'(\mathbf{w})$ denote the gradient of the total error with respect to the weight vector $\mathbf{w}$, $\mathbf{p}_k$ the conjugate search direction at iteration k and λ_k, σ_k scalar parameters. The vector $\mathbf{s}_k$ is computed as:

$$\mathbf{s}_k = \frac{\mathbf{E}'(\mathbf{w}_k + \sigma_k \mathbf{p}_k) - \mathbf{E}'(\mathbf{w}_k)}{\sigma_k} + \lambda_k \mathbf{p}_k \tag{3}$$

The first term is a finite-difference approximation of the Hessian applied to the direction $\mathbf{p}_k$, i.e., $H_k \mathbf{p}_k$, while the second term $\lambda_k \mathbf{p}_k$ introduces a damping component to ensure positive definiteness of the Hessian approximation. Both terms are vectors of the same dimension as $\mathbf{w}_k$, ensuring dimensional consistency in the update computation.

In this formulation, the first term provides a finite-difference approximation to the curvature term $\mathbf{E}''(\mathbf{w}_k) \cdot \mathbf{p}_k$, allowing SCG to incorporate second-order information without explicitly computing the Hessian. This enables adaptive step size and direction updates without costly line searches, resulting in stable and efficient convergence, particularly well suited for medium-scale problems such as neural data classification.

To enhance the reliability of the results, a 10-fold cross-validation is used (Kordos & Duch, 2008; Paul & Karn, 2023). The data set is randomly divided into 10 groups (folds). In each iteration, one group is used as the test set, while the remaining nine groups are used for training. This ensures a robust evaluation of the model's generalization performance across all data subsets.

Implementation and training were performed using MATLAB 2024b in this study. The built-in function *patternnet* was used to construct a feed-forward neural network that supports the classification of multichannel data and is suitable for supervised learning tasks. This tool simplifies the development of neural networks by handling data formatting, training configuration, and evaluation internally.

In this thesis, we designed two separate ANN models to classify EEG data based on different input representations: signal space and source space. In the signal space model, the EEG epochs consisted of raw time-series data from 19 channels, each with 200 time points, resulting in an input size of 3800 (19 x 200) per sample. This data was flattened and used as direct input to a feed-forward ANN with 3800 input neurons, one hidden layer of 10 neurons, and a single output neuron for binary classification (spike vs. non-spike).

In contrast, the source space model used a reduced representation with an input dimension of 200 per sample, reflecting processed or localized brain source signals.

This version of the ANN had a simpler structure, with 200 input neurons feeding into classification.

Both architectures used activation functions and were trained using the SCG algorithm. The visual representations of each ANN structure are provided in Figures 12 to illustrate the differences in model design and data flow.

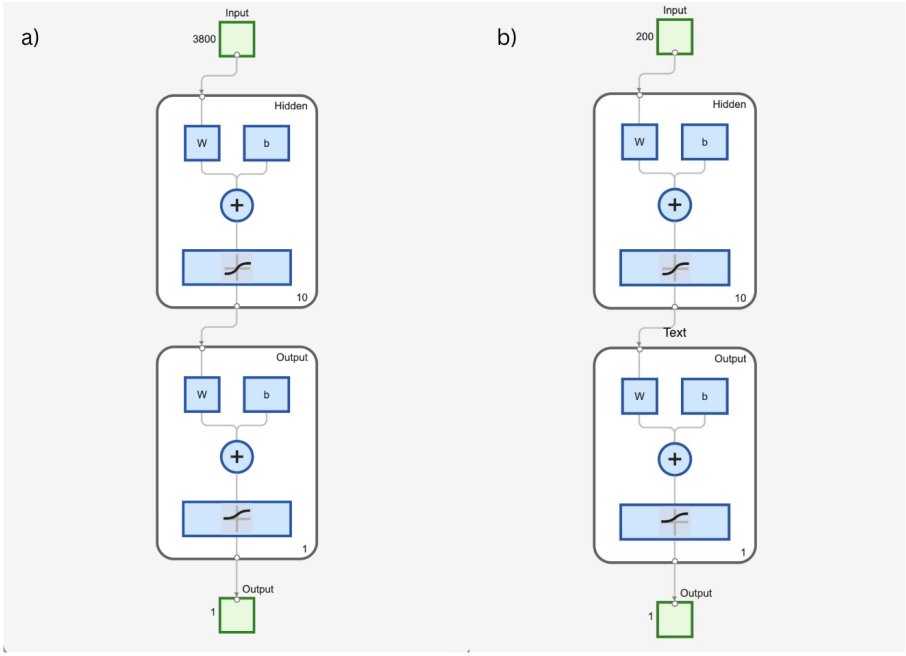

Figure 12
ANN architecture a) Signal space: 3800 input features (19 channels x 200 time points), 10 hidden neurons, and a single binary output. **b)** Source space: 200 input features, 10 hidden neurons, and a single binary output. Here W denotes the layer's weight matrix, b denotes the bias vector, and the 'TEXT' label is a placeholder with no functional meaning.

Evaluation Metrics

The performance of the model was evaluated using standard classification metrics: accuracy, sensitivity, specificity, precision, F1 score, geometric mean, Cohen's Kappa, and area under the ROC curve (AUC-ROC). Collectively, these metrics present a multidimensional evaluation framework. While accuracy offers a coarse view of overall performance, sensitivity and specificity address class-wise performance; precision and the F1 score provide insight into the correctness and balance of positive predictions; and the geometric mean, Cohen's Kappa, and AUC-ROC further refine the assessment by addressing issues such as imbalance, chance agreement, and threshold-independence. This integrated approach ensures that model

evaluation is both rigorous and appropriately tailored to the nuances of the application domain (Pattanayak et al., 2024; Simbun & Kumar, 2025; Wang & Carvalho, 2024).

2.8 Feature extraction

Feature extraction is a fundamental step in EEG analysis, aiming to transform high-dimensional raw signals into informative representations that emphasize relevant signal characteristics while reducing redundancy and noise (Beutel et al., 2000). In this thesis, feature extraction played a key role in preparing EEG data for the detection of epileptic spikes using ANNs.

EEG data, recorded from 19 EEG channels, were segmented into 1-second epochs, each with dimensions of 19 × 200 (channels × time points) and the datasets were maintained for each expert annotation set (EP1, EP2, EP3) as mentioned in the previous sections.

Features were extracted from both signal space and source-space data.

2.8.1 Amplitude-Based Features

Amplitude-based features capture the fundamental distributional characteristics of the EEG signal by quantifying statistical properties (Boubchir et al., 2017). The mean amplitude $\bar{x}$ represents the average signal level over the recording interval, serving as a baseline indicator of the overall electrical activity (Sanei & Chambers, 2007).

$$\bar{x} = \frac{1}{N} \sum_{i=1}^{N} x_i \tag{4}$$

Standard deviation σ measures the variability around this mean, reflecting fluctuation due to neural dynamics or noise (Boonyakitanont et al., 2020).

$$\sigma = \sqrt{\frac{1}{N} \sum_{i=1}^{N} (x_i - \bar{x})^2} \tag{5}$$

Skewness S quantifies the asymmetry of the amplitude distribution, which may indicate bias or an imbalance in the underlying brain activity (Rousseau et al., 2018), while kurtosis K evaluates the 'tailedness' or peakedness, highlighting the presence of extreme values that could correspond to transient events or artifacts.

Formula of Skewness:

$$S = \frac{\frac{1}{N}\sum_{i=1}^{N}(x_i - \bar{x})^3}{\left(\frac{1}{N}\sum_{i=1}^{N}(x_i - \bar{x})^2\right)^{3/2}} \tag{6}$$

Formula of Kurtosis:

$$K = \frac{\frac{1}{N}\sum_{i=1}^{N}(x_i - \bar{x})^4}{\left(\frac{1}{N}\sum_{i=1}^{N}(x_i - \bar{x})^2\right)^{2}} \tag{7}$$

Values of $K > 3$ suggest heavy tails (leptokurtic), while $K < 3$ indicates light tails (platykurtic). These statistical descriptors are commonly used to identify abnormal patterns such as seizure-like activity (Rousseau et al., 2018).

2.8.2 Nonlinear Dynamics Features

Nonlinear dynamics features assess the complex, often chaotic nature of EEG signals. These features quantify how signal patterns change across time and scale, offering insights into the underlying neural dynamics (Larsson, 2018).

The Higuchi Fractal Dimension (HFD) is a robust measure used to determine the self-similarity and scaling behavior of a time series across multiple resolutions. It effectively captures the fractal characteristics of brain activity (Larsson, 2018). The EEG time series is first sub-sampled into k datasets:

$$x_k(m) = \{x(m), x(m+k), x(m+2k), \ldots, x\left(m + \left\lfloor \frac{N-m}{k} \right\rfloor \cdot k\right)\} \tag{8}$$

Here, $\lfloor \cdot \rfloor$ denotes the floor function, k is the interval time with values $k = 1, 2, 3, \ldots, k_{\max}$, and m is the initial time with values $m = 1, 2, 3, \ldots, k$. For EEG data $k_{\max}$ is typically set to $\lfloor \frac{N}{2} \rfloor$, where N is the total number of samples (Ruiz de Miras, 2016).

For each fixed k, the curve length $L_k(m)$ is computed as the sum of the absolute differences between consecutive sub-sampled points, normalized for the scaling of sub-series (Güven et al., 2020):

$$L_k(m) = \frac{\sum_{i=1}^{\lfloor \frac{N-m}{k} \rfloor} |x(m+ik) - x\left(m+(i-1)k\right)| \cdot \frac{N-1}{\lfloor \frac{N-m}{k} \rfloor \cdot k}}{k} \tag{9}$$

The average curve length for a given k is then:

$$HFD_k = \frac{1}{k}\sum_{m=1}^{k} L_k(m) \tag{10}$$

The Hinguchi Fractal Dimension D_H is obtained as the slope of the regression line in the log-log plot of $\ln(HFD_k)$ versus $\ln(1/k)$. This means that for each k, the relationship $HFD_k \propto k^{-D_H}$ holds, and the exponent D_H quantifies the fractal scaling of the EEG signal.

Choosing small k values makes $L_k(m)$ effectively a measure of signal length, meaning sharp transients or spikes will increase its value. Larger k values capture coarser structural patterns in the signal.

In contrast, Katz Fractal Dimension (KFD) relates the total path length of the signal to its overall spatial extent, providing insight into the degree of morphological complexity (Larsson, 2018). For EEG time series x_i with N points, the total length L of the signal is defined as the sum of Euclidean distances between successive points:

$$L = \sum_{i=1}^{N-1} \sqrt{1 + (x_{i+1} - x_i)^2} \tag{11}$$

This value reflects the cumulative "travel distance" of the signal and serves as a measure of its irregularity.

This signal diameter d is defined as the maximum Euclidean distance between the first point $(1, x_1)$ and any other point (i, x_i) in the series:

$$d = \max_{2 \le i \le N} \sqrt{(1 - i)^2 + (x_1 - x_i)^2} \tag{12}$$

This captures the largest spatial extent of the signal trajectory. The Katz Fractal Dimension is then calculated as:

$$D_K = \frac{\log(N)}{\log(N) + \log\left(\frac{L}{d}\right)} \tag{13}$$

Here, N is the total number of points in the series, L quantifies the total path length, and d represents the maximum distance from the starting point.

Additionally, the Lyapunov (F4) exponent λ quantifies the rate at which the nearby trajectories in the reconstructed phase space diverge, thereby offering an index for the level of chaos or instability exhibited by the EEG signal (Rüdisüli et al., 2013). A positive λ implies sensitivity to initial conditions and chaotic dynamics, while negative or zero values indicate stability.

Given a time series x_i, an initial perturbation ϵ is applied to form a perturbed trajectory. If x_i^n denotes the i-th point after n iterations, the divergence rate is given

by:

$$\frac{x_{i+\varepsilon}^{n} - x_{i}^{n}}{\varepsilon} \tag{14}$$

For infinitesimally small ϵ, this becomes proportional to the complexity of the system:

$$\lambda = \lim_{\varepsilon \to 0} \frac{1}{n} \frac{x_{i+\varepsilon}^{n} - x_{i}^{n}}{\varepsilon} \tag{15}$$

Applying the chain rule, λ can also be expressed as:

$$\lambda = \lim_{n \to \infty} \frac{1}{n} \sum_{i=1}^{n-1} \ln |x_{i}'| \tag{16}$$

These measures have been instrumental in characterizing the nonlinear dynamics that often signal pathological conditions such as epilepsy (Lehnertz, 2008).

2.8.3 Frequency-Based Features

Frequency-based features derive from spectral analysis and are crucial for characterizing oscillatory brain activity.

Power Spectral Density (PSD; F5a, F5b, F5c) is a central metric that shows how the power of the EEG signal is distributed over different frequency components, computed using techniques such as the periodogram or Fourier transform (Zhao et al., 2019). The EEG is typically subdivided into clinically relevant frequency bands. Within these, delta (0.5–4 Hz), theta (4–8 Hz) and alpha (8–13 Hz) are important for capturing slow-wave components, while beta (13–30 Hz) and gamma (30–60 Hz) bands capture faster oscillatory processes (Ameera et al., 2019). Specific combined feature sets (F5a, F5b, F5c) enable targeted analysis of neural oscillations that correlate with various cognitive and pathological states (Wang et al., 2017).

2.8.4 Entropy-Based Features

Entropy-based features quantify the irregularity, predictability, and information content of the signal. Approximate Entropy (F10, see Table 6 for feature numbering to clarify the jump from F5 to F10) quantifies the logarithmic likelihood that sequences of m consecutive data points, which are similar within a tolerance r, remain similar when extended. Lower values indicate more regular, predictable signals, while higher values indicate greater irregularity and complexity. Shannon Entropy (F12), on the other hand, calculates the average uncertainty inherent in a signal's probability distribution by assessing its informational content. These entropy measures are particularly valuable in delineating the differences between normal and

abnormal brain states, as changes in signal complexity have been linked to various neurological conditions (Uyulan et al., 2019).

Combined feature sets integrate these diverse descriptors to form richer, multidimensional representations of the EEG data. They enhance classification performance by leveraging complementary information from amplitude, nonlinear, frequency and entropy domains, making them especially useful in applications such as epileptic seizure detection (Akter et al., 2020).

3 Results

This section presents the results of the ANN classification for the four conditions outlined in Table 4. The primary objective was to evaluate the impact of different data representations, ranging from raw signal space EEG to feature-extracted source localized activity, on the automated identification of IEDs.

The classification performance for each condition is reported using key metrics such as accuracy, sensitivity, and specificity to provide a robust assessment of the ANN's capabilities. Initially, we detail the performance achieved using data from signal space (Conditions 1 and 2). Subsequently, we present the results from the source-localized data (Conditions 3 and 4), followed by a comparative analysis across all conditions to highlight the advantages of source space processing for ANN-based IED detection.

Table 4

Four Distinct Conditions for Artificial Neural Network (ANN) Classification. Each condition specifies the type of input data used for training and evaluating the ANN model.

Condition	**Input data**
1. Signal Space (Raw)	Raw EEG epochs (signal space)
2. Signal Space (Features extracted)	Features extracted from signal space
3. Source Space (Raw)	Raw Source-Localized Epochs
4. Source Space (Features extracted)	Features extracted from source space

3.1 Signal Space Analysis Without Feature Extraction

This section presents the results of the artificial neural network (ANN) classification applied to raw EEG data (Condition 1) in the signal space, without any feature extraction. EEG recordings were segmented into 1-second epochs, and each

epoch, originally in a `[19 × 200]` matrix format, was reshaped into a `[1 × 3800]` feature vector to be used as input to the ANN.

A feedforward neural network (FFNN) with a single hidden layer comprising 10 neurons was used, as described in Section 2.7. Training was performed using the SCG backpropagation algorithm with a maximum of 500 epochs per fold, and early stopping was enabled to prevent overfitting. The network was trained and evaluated using 10-fold stratified cross-validation, meaning the model was retrained from scratch for each fold. Classification performance was assessed using several commonly reported metrics, including accuracy, sensitivity (recall), specificity, precision, F1 score, geometric mean (G mean), and Cohen's Kappa.

The classification performance on the raw EEG epochs is summarized in Table 5.

Table 5
Averaged ANN classification results for raw signal space data using AND-marking and OR-marking.

Metric	**AND-marking**	**OR-marking**
Accuracy	0.521	0.512
Sensitivity	0.428	0.498
Specificity	0.613	0.525
Precision	0.526	0.512
F1-score	0.472	0.505
G-Mean	0.513	0.511
Cohen's Kappa	0.042	0.024

These results serve as a baseline for evaluating the impact of feature extraction and source-space transformation in subsequent sections. The overall classification accuracies for both AND-marking (0.521) and OR-marking (0.512) are very close, indicating that the ANN struggled to effectively distinguish between spike and non-spike events based solely on raw EEG data. This is further corroborated by the low Cohen's Kappa values (0.042 for AND marking and 0.024 for OR marking), which suggest that the agreement between the ANN's predictions and the true labels is negligible, only marginally better than random assignment.

For the AND-marking strategy, the sensitivity (0.428) indicates that less than half of the actual spike events were correctly identified, while specificity (0.613) shows a slightly better ability to correctly identify non-spike events. The OR-marking strategy, in contrast, exhibits a more balanced, still low performance sensitivity (0.498) and specificity (0.525). These findings clearly underscore the need for more discriminative features or alternative data representations to improve generalization and achieve clinically meaningful performance in automated IED detection.

3.2 Signal Space Analysis with Feature Extraction

To evaluate the effect of feature engineering on the classification of interictal epileptiform discharges (IEDs), various handcrafted features were extracted from preprocessed EEG epochs in signal space and used as input (Condition 2). Each feature set, as detailed by its ID, was used to train and evaluate a separate feedforward neural network. The network architecture and training parameters remained consistent with those used in Condition 1.

Table 6

ANN Classification Performance for AND-Marked Signal Space Features.Averaged Accuracy, Sensitivity, and Specificity for various feature sets (ID F1-F12) using the AND-marking strategy.

Feature ID	Accuracy	Sensitivity	Specificity
F1 (Statistical)	0.94	0.95	0.94
F2 (Katz FD)	0.98	0.99	0.97
F3 (Higuchi FD)	0.87	0.88	0.86
F4 (Lyapunov Exponent)	0.91	0.92	0.90
F5a (PSD, gamma, beta)	0.85	0.86	0.85
F5b (PSD, all bands)	0.94	0.96	0.93
F5c (PSD, alpha delta theta)	0.88	0.91	0.84
F6 (F5a + F2 + F1)	0.98	0.98	0.97
F7 (F5a + F2 + F1 +F4)	0.97	0.98	0.97
F8 (F2 + F4)	0.98	0.98	0.97
F9 (F1 + F2)	0.97	0.97	0.97
F10 (Approximate Entropy)	0.92	0.93	0.92
F11 (F2 + F10)	0.97	0.97	0.97
F12 (Shannon Entropy)	0.87	0.89	0.85

The results presented in Table 6 and Table 7 clearly demonstrate a significant improvement in ANN classification performance when utilizing feature-extracted data compared to the raw EEG signals (Condition 1).

For the AND-marking strategy, where an epoch was labeled as a spike only if all three epileptologists agreed on its presence, several feature sets, including F2 (Katz Fractal Dimension), F6 (a combination of F5a, F2, and F1), F7, F8, F9, and F11 achieved exceptional performance with accuracies of 0.97 or higher. These feature sets also maintained consistently high sensitivity and specificity, indicating a balanced ability to correctly identify both spike and non-spike events.

For the AND-marking strategy, the Katz Fractal Dimension (F2) and several combined feature sets achieved accuracies of 0.97 or higher, with balanced sensitivity

and specificity.

Table 7

ANN Classification Performance for OR-Marked Signal Space Features. Averaged Accuracy, Sensitivity, and Specificity for various feature sets (ID F1-F12) using the OR-marking strategy.

Feature ID	Accuracy	Sensitivity	Specificity
F1 (Statistical)	0.84	0.87	0.81
F2 (Katz FD)	0.88	0.94	0.83
F3 (Higuchi FD)	0.68	0.66	0.70
F4 (Lyapunov Exponent)	0.77	0.79	0.76
F5a (PSD, gamma, beta)	0.74	0.77	0.72
F5b (PSD, all bands)	0.69	0.51	0.88
F5c (PSD, alpha delta theta)	0.62	0.33	0.91
F6 (F5a + F2 + F1)	0.89	0.92	0.86
F7 (F5a + F2 + F1 +F4)	0.90	0.93	0.87
F8 (F2 + F4)	0.89	0.94	0.83
F9 (F1 + F2)	0.90	0.93	0.88
F10 (Approximate Entropy)	0.80	0.80	0.80
F11 (F2 + F10)	0.89	0.94	0.85
F12 (Shannon Entropy)	0.67	0.51	0.83

For the OR-marking strategy (Table 7), where an epoch was labeled as a spike if at least one of the three epileptologists identified it as such, a general improvement over raw data is observed. However, the peak performance is slightly lower and there is more variability across features compared to AND-marking. The highest accuracies for OR-marking (0.88-0.90) were achieved by feature sets such as F2, F6, F7, F8, F9 and F11. In particular, F2 (KFD) achieved an accuracy of 0.88 for OR-marking with a high sensitivity of 0.94, suggesting good detection of actual spikes, but a slightly lower specificity of 0.83 compared to its AND-marking counterpart (0.97). This observed difference in performance between two marking strategies is directly attributable to their underlying definition. The AND-marking set represents highly stereotypical and clear IEDs due to the strict consensus requirement, making them easier for the ANN to learn and classify with high precision. In contrast, the OR-marking set encompasses a broader, more heterogeneous range of events, including those with less clear morphology or inter-rater agreement. This increased variability and potential inclusion of events in the OR-marking set likely contribute to its slightly reduced overall accuracy and greater fluctuations in performance across different feature sets.

Beyond accuracy, sensitivity and specificity, other evaluation metrics such as pre-

cision, F1-score, Geometric mean, and Cohen's kappa were also computed to provide a comprehensive performance assessment. The top-performing feature sets, as identified by their high accuracies in both marking strategies, generally also yielded excellent F1-scores (ranging from approximately 0.87 to 0.98 for AND-marking and above 0.70-0.80 for OR-marking's best features), indicating substantial to almost perfect agreement with the true labels and a vast improvement over raw data performance.

Conversely, feature sets like F5c (PSD: alpha, delta, theta) and F12 (Shannon Entropy) frequently showed lower overall performance for both strategies, particularly for OR-marking. For these less discriminative features, the F1-scores dropped to approximately 0.50-0.70, and Cohen's kappa values were correspondingly lower (e.g., F5c OR-marking Kappa around 0.24, F12 OR-marking Kappa around 0.35), although still significantly better than raw data. These findings highlight the profound impact of appropriate feature engineering in transforming near-chance performance into robust IED classification. Notably, in both results and those reported by Yeşilbaş et al., 2023, KFD alone achieved performance levels close to the best feature combinations, suggesting that KFD is the primary driver of high accuracy, while combinations offer only marginal additional benefit.

3.3 Source Space Analysis without Feature Extraction

This subsection outlines the classification methodology applied to source-localized EEG data, aiming to improve the signal-to-noise ratio for classification. The objective of this analysis was to evaluate if source-level representation of neural activity could support robust classification of spike events. Two distinct source models were investigated: a fixed orientation model and a free orientation model, which was described in Section 2.5.5.

The fixed orientation model constrains the dipole moment at each cortical node to a single direction, resulting in a single degree of freedom (DOF) per node. This simplifies the problem but may not accurately capture the true orientation of the neural sources. In this model, a solution for a patch with K nodes yields a source vector of dimension $K \times T$.

The free orientation model provides a more flexible solution by allowing the dipole moments to have three independent components (x, y, z), corresponding to three degrees of freedom per node. This results in a source vector of dimension $3K \times T$. The free-orientation model is expected to provide a more accurate fit to the EEG data but is more susceptible to noise and requires careful regularization (Makkonen, 2023).

The classification performance for both source space models is summarized in Table 8.

Table 8
ANN classification results for source-space data using fixed- and free-orientation models.

Metric	**AND**		**OR**	
	Fixed orient.	**Free orient.**	**Fixed orient.**	**Free orient.**
Accuracy	0.5375	0.5958	0.5116	0.5872
Sensitivity	0.6002	0.5799	0.6614	0.6263
Specificity	0.4748	0.6116	0.3617	0.5480
Precision	0.5333	0.5989	0.5089	0.5809
F1-score	0.5648	0.5892	0.5752	0.6027
G-Mean	0.5338	0.5956	0.4891	0.5859
Cohen's Kappa	0.5374	0.1915	0.5115	0.1744

As shown in Table 8, for the AND-marking strategy in the source space (Condition 3), the fixed orientation model achieved an accuracy of 0.5375. While this represents a marginal improvement over the raw signal space data (Condition 1), it still suggests that using raw source-localized data without feature extraction is insufficient for robust IED detection. The sensitivity was 0.60, indicating that a higher proportion of actual spike events were identified compared to the raw signal space. However, the specificity was lower at 0.47, meaning a reduced ability to correctly identify non-spike events. The F1 score of 0.56 and Cohen's Kappa of 0.53, while better than the raw signal space, still suggest only a fair to moderate agreement with the true labels, highlighting the limitations of relying solely on raw source waveforms for classification.

For the free orientation model using the AND marking strategy, the ANN achieved an accuracy of 0.5958. This represents a substantial improvement over the fixed orientation model and the raw signal space data. The sensitivity was 0.5799, and the specificity was 0.6116, indicating a better balance between detecting true positive and true negative events compared to the fixed orientation model. The F1-score of 0.5891 and G-Mean of 0.5956 further demonstrate the improved performance of the free orientation model, as these metrics provide a more balanced view of performance on imbalanced datasets.

For the OR-marking strategy in the source space (Condition 3), the ANN achieved an accuracy of 0.51. This performance is very similar to that observed for raw signal space data with OR-marking (Table 5), suggesting that fixed orientation alone does

not significantly improve classification for the OR-marked IEDs. The sensitivity for OR marking in source space was 0.66, indicating a relatively good ability to detect actual spike events. In this OR marking, a "false positive" refers to a non-spike event that was incorrectly classified as a spike. A true spike event in the OR condition is defined as a time point where at least one of the three epileptologists identified a spike. However, this came at the cost of a lower specificity of 0.36, implying a high rate of false positives. The F1 score of 0.57 and Cohen's Kappa of 0.51, while slightly higher than their raw signal space counterparts, still reflect a limited overall performance and highlight the challenges of classifying diverse IEDs without the aid of specific features, even when leveraging source-level information provided by a one-degree-of-freedom fixed dipole model.

For the free-orientation model with the OR marking strategy, the ANN achieved an accuracy of 0.5872, representing a notable improvement over the fixed-orientation model. The sensitivity was 0.6263 and the specificity was 0.5480, indicating a more balanced classification performance than the fixed-orientation model. The F1-score of 0.6027 and G-mean of 0.5859 suggest that the free-orientation model, which provides three source waveforms per node, contains more detailed information that the ANN can successfully leverage for classification compared to the fixed-orientation model.

3.4 Source Space Analysis with Feature Extraction

This section evaluates the performance of the ANN when trained on feature-extracted data from the source space, which is the last condition. The objective was to determine whether combining the spatial specificity of source localization with the feature extraction could further enhance IED classification accuracy.

For the AND-marking strategy in the source space, the results presented in Table 9 demonstrate a notable improvement in classification performance compared to using raw source-localized data (Condition 3). The fixed-orientation model consistently outperforms the free-orientation model across feature sets. The highest accuracy for the fixed-orientation model was 0.84 (F1, F6, F7), while the highest for the free-orientation model was 0.75 (F2). These top-performing feature sets also exhibited a good balance between sensitivity and specificity, indicating their effectiveness in correctly identifying both spike and non-spike events.

Further analysis reveals that statistical features (F1) alone demonstrated significant discriminative power, achieving an accuracy of 0.84 with a sensitivity of 0.81 and a specificity of 0.86 under the fixed-orientation model. This strong performance implies that the source localization process effectively filters out much of the back-

Table 9

ANN Classification Performance for AND-Marked Source Space Features under fixed- and free-orientation models. Averaged Accuracy, Sensitivity, and Specificity for various feature sets (ID F1–F12).

Feature ID	**Accuracy**		**Sensitivity**		**Specificity**	
	Free	**Fixed**	**Free**	**Fixed**	**Free**	**Fixed**
F1 (Statistical)	0.70	0.84	0.69	0.81	0.72	0.86
F2 (Katz FD)	0.75	0.68	0.76	0.62	0.75	0.73
F3 (Higuchi FD)	0.57	0.62	0.68	0.72	0.46	0.51
F4 (Lyapunov Exponent)	0.61	0.59	0.59	0.65	0.64	0.52
F5a (PSD, gamma, beta)	0.60	0.77	0.69	0.67	0.50	0.86
F5b (PSD, all bands)	0.62	0.78	0.88	0.72	0.36	0.85
F5c (PSD, alpha delta theta)	0.54	0.59	0.94	0.75	0.14	0.43
F6 (F5a + F2 + F1)	0.74	0.84	0.72	0.81	0.75	0.87
F7 (F5a + F2 + F1 +F4)	0.73	0.84	0.73	0.83	0.72	0.85
F8 (F2 + F4)	0.72	0.66	0.69	0.66	0.75	0.66
F9 (F1 + F2)	0.73	0.83	0.71	0.82	0.75	0.85
F10 (Approximate Entropy)	0.61	0.61	0.61	0.63	0.60	0.59
F11 (F2 + F10)	0.73	0.69	0.72	0.69	0.74	0.68
F12 (Shannon Entropy)	0.65	0.63	0.77	0.80	0.52	0.45

ground noise. The rising flank of an IED, which has a stable EEG topography, projects a distinct and "peaky" waveform onto the source space whose statistical features are well-suited to capture. This finding highlights that for a fixed dipole orientation, simple statistical measures are often sufficient.

However, a critical trade-off is observed when comparing these results to the signal space analysis. Several features showed considerably lower performance in source space, most notably F2 (Katz FD), which dropped from 0.98 accuracy in signal space to 0.68 in the fixed-orientation model. The peak accuracies in source space are also generally lower than those from the best-performing feature sets in signal space. This indicates that while source localization provides a spatially refined signal, the process may discard or alter some of the spatiotemporal complexity that features like F2 are designed to capture. This is likely due to the simplified nature of the source model, where projecting a complex multi-channel signal to a signal source waveform acts as a significant data compression.

Interestingly, this effect was not as strong for the free orientation (3D) model, where F2 performed better (0.76 accuracy) than in the fixed orientation model (0.68 accuracy). This supports the hypothesis that allowing for variable dipole

orientations (three free parameters per source location) retains more of the signal's complexity and thus better preserves the discriminative power of certain features.

Table 10

ANN Classification Performance for OR-Marked Source Space Features under fixed- and free-orientation models. Averaged Accuracy, Sensitivity, and Specificity for various feature sets (ID F1–F12).

Feature ID	**Accuracy**		**Sensitivity**		**Specificity**	
	Free	**Fixed**	**Free**	**Fixed**	**Free**	**Fixed**
F1 (Statistical)	0.59	0.65	0.56	0.55	0.63	0.74
F2 (Katz FD)	0.60	0.59	0.72	0.59	0.49	0.60
F3 (Higuchi FD)	0.56	0.59	0.64	0.67	0.47	0.52
F4 (Lyapunov Exponent)	0.57	0.57	0.50	0.60	0.63	0.53
F5a (PSD, gamma, beta)	0.51	0.50	0.70	0.37	0.31	0.63
F5b (PSD, all bands)	0.52	0.50	0.90	0.65	0.15	0.36
F5c (PSD, alpha delta theta)	0.51	0.51	0.73	0.64	0.30	0.37
F6 (F5a + F2 + F1)	0.59	0.64	0.57	0.59	0.62	0.70
F7 (F5a + F2 + F1 +F4)	0.61	0.65	0.57	0.59	0.65	0.71
F8 (F2 + F4)	0.57	0.58	0.51	0.58	0.64	0.59
F9 (F1 + F2)	0.60	0.65	0.58	0.57	0.63	0.73
F10 (Approximate Entropy)	0.57	0.56	0.58	0.62	0.57	0.50
F11 (F2 + F10)	0.57	0.58	0.57	0.61	0.57	0.55
F12 (Shannon Entropy)	0.53	0.53	0.82	0.88	0.24	0.16

The OR marking strategy, where a spike is labeled if at least one epileptologist identified it, results in a more diverse compared to the AND marking strategy. Table 10 presents the classification performance of the various feature sets under this condition.

Overall, classification accuracy across most feature sets decreased when using OR-marked data. The highest accuracy was by F1, F7 and F9, each reaching an accuracy of 0.65 under the fixed-orientation model. These feature sets also maintained relatively balanced sensitivity and specificity, suggesting that statistical and mixed-domain features retain some discriminative ability even under less consistent labeling.

As with the AND-marked data, the fixed-orientation model generally outperformed the free-orientation model. The highest accuracy for the fixed model was 0.65, while the highest for the free model was 0.60. This further supports the hypothesis that constraining the dipole orientation to a single, physiologically plausible direction helps to reduce noise and enhance the stability of the signal, which

is especially true in a more challenging, ambiguous dataset.

However, the sensitivity values across most features remained modest, typically below 0.65, indicating challenges in correctly identifying all spike events when the labeling is based on partial expert agreement. This was particularly evident with the PSD-based feature sets. These showed low specificity and unbalanced performance, indicating a tendency towards false positives.

Conversely, some features performed poorly under OR-marking, demonstrating limited robustness in the dataset. Shannon Entropy exhibited very high sensitivity (0.88) but a low specificity (0.16), rendering it unsuitable for reliable classification due to an excessive number of false positives. Similarly, Approximate Entropy (F10) and F11 showed low accuracies.

These results emphasize that while feature extraction in source space can improve classification compared to raw source data, the benefit is heavily influenced by the consistency of the labeling strategy. The OR-marking, by incorporating more ambiguous and subjective spike events, introduces variability that significantly impacts model performance. The lower overall performance, even for top features like F1, suggests that the OR-marked dataset contains more events that are not well-represented by a single, simple source model. This supports the idea that the "1-parameter projection" may be too simplistic for a dataset with such higher inter-rater variability, as the additional complexity of the OR-marked events might be lost.

4 Discussion

4.1 Summery of key findings

This thesis aimed to systematically evaluate the impact of different EEG data representations on the automated identification of interictal epileptiform discharges (IEDs) using Artificial Neural Networks (ANNs). The primary objective was to examine how different EEG data conditions affect the ANN's ability to accurately classify spike events. The findings show a distinct pattern of performance across the four conditions, underscoring the critical role of appropriate data preprocessing and feature extraction in achieving robust and meaningful IED detection.

The initial analysis, using raw EEG data in signal space (C1), demonstrated very limited classification capability, with accuracy and sensitivity values close to chance level (Table 5). Cohen's Kappa was particularly low, suggesting poor agreement between predicted and true labels. These findings confirm that the raw EEG

data lacks sufficient structure for IED classification without any feature extraction. Importantly, prior work by Yeşilbaş et al., 2023 showed that restricting the analysis to the 12 most informative bipolar channels from the standard 19 electrodes already led to substantially better results, with ANN models reaching 0.72 accuracy for both AND-marking and OR-marking. This contrast highlights that even modest preprocessing steps, such as electrode selection, can considerably improve the detectability of spike-related patterns, bridging the gap between noisy raw signals and meaningful neural representations.

The second condition (C2) shows the highest overall performance in the study. Feature extraction strongly enhanced classification with several feature sets, particularly Katz Fractal Dimension (F2) and its combinations with statistical and PSD features, which are F6, F7, F9, and F11, resulting in classification accuracies of 0.97 for AND marking data (Table 6). Notably, Katz FD alone was dominant, consistent with Yeşilbaş et al., 2023 findings that it best represented interictal spikes across both AND and OR marked datasets. Even for the OR marking strategy, where at least one epileptologist agreed on the spike event, feature-based models achieved accuracies above 0.88 (Table 7). Sensitivity, specificity and F1 scores increased as well, indicating the presence of a relevant feature pattern for neural classification. These results reinforce that carefully chosen nonlinear and spectral descriptors capture relevant EEG dynamics that enable robust ANN-based IED detection.

The third condition (C3), where the raw source localized data was used, offered only marginal improvements over signal space input. As shown in Table 8 free-orientation model slightly improved accuracy (0.60 for AND marking, 0.59 for OR marking) compared to fixed-orientation models (0.54 and 0.51, respectively). Sensitivity was somewhat higher in both marking strategies, but specificity remained low, particularly for OR marking (0.36 with fixed orientation). This imbalance suggests that the ANN was prone to false positives in this setting. Cohen's Kappa and F1-score were higher than in Condition 1, indicating that source projection contributed some structure to the data. However, the overall performance remained moderate and far below the levels achieved with explicit feature extraction (C2). It is important to note that these findings apply specifically to the examined 1-parameter source projection approach. More sophisticated source-space models, such as multi-parameter reconstruction, might offer stronger benefits. Within the current framework, however, source projection alone provided only limited improvements for automated IED detection.

Lastly, the fourth and final condition (C4), feature extraction, was applied to the source space. For the AND-marking strategy, combined and single feature sets

achieved up to 0.84 accuracy. However, these results did not outperform the model in signal space (C2). This suggests that the simplified source model loses valuable spatiotemporal information. The performance drop of features like F2 is possibly due to the polarity of the data, for example, if the pattern rotates or changes due to activity propagating from the sulcal valley to the gyral crown. The free-orientation (3-parameter) model's better performance for F2 supports this, as it retains more of the signal's complexity. For OR marking, the performance with feature extraction presented additional challenges. While some individual and combined feature sets still offered improved accuracy compared to the raw data, overall performance for this marking remained lower than what was achieved with AND marking.

4.2 Interpretation of Signal Space results

The analysis of signal space EEG data under two distinct processing conditions, which are condition 1 (raw input) and condition 2 (using feature extraction), revealed a contrast in classification performance, providing important insights into the role of signal representation in automated IED detection.

In raw input, where EEG epochs were directly used as vectors and fed into the ANN, the network demonstrated poor classification, with low accuracy around 52%̇These findings suggest that raw EEG data may be too noisy and redundant to be effectively leveraged by a simple feedforward neural network without prior transformation. The lack of structure in the raw signals likely led to poor generalization and high misclassification rates, particularly in differentiating IED patterns. Importantly, earlier work by Yeşilbaş et al., 2023 showed that even a modest reduction in electrode count (from 19 standard electrodes down to 12 carefully selected bipolar channels) already improved ANN performance considerably, with accuracies of 0.70 for both AND and OR marking conditions. This contrast highlights that electrode selection and dimensionality reduction alone can substantially enhance spike detectability, even before applying explicit feature extraction.

In contrast, condition 2 demonstrated a marked improvement in performance across nearly all metrics after applying feature extraction. This method captured key morphological and spectral characteristics of IEDs, allowing the ANN to more effectively distinguish spike from non-spike events. Notably, Katz Fractal Dimension (KFD) alone was the dominant feature, achieving high accuracies under AND-marking. The combination of fractal and spectral features (e.g., F6, F7, F9, F11) further boosted classification, reflecting the complementary nature of nonlinear and frequency-based descriptors. Beyond high accuracy, the feature-extracted dataset also achieved strong sensitivity and specificity, underscoring the robustness of this

representation.

The consistently high performance with AND-marked data reflects the utility of labeled clear-cut IEDs for training reliable models. Meanwhile, the slightly reduced and more variable performance under OR marking emphasizes the challenge posed by more spike morphologies. This difference is primarily attributable to the underlying definition of the datasets: the AND marking dataset consists of only those events where all epileptologists unanimously agreed on a spike, resulting in a smaller, more uniform and highly stereotypical set of IEDs. While the OR marking dataset includes any event identified as a spike by at least one epileptologist, leading to a larger, more diverse and potentially ambiguous set of data points. Nonetheless, the feature-based condition in signal space still performed well even in this noisier labeling scenario.

Importantly, the signal space results underscore that data representation is foundational to successful EEG classification. While raw signal input offers the full temporal structure of EEG, it lacks the abstraction necessary for pattern recognition by neural networks. Feature extraction methods, on the other hand, serve as both dimensionality reduction and noise suppression strategies, enabling the ANN to exploit discriminative signal properties. The comparison with Yeşilbaş et al., 2023 12-electrode study further highlights that reducing irrelevant input dimensions, whether by channel selection or by extracting higher-level features, is essential for building reliable automated IED detection.

4.3 Interpretation of Source Space results

The evaluation of source-localized EEG data (C3, C4) aimed to determine whether operating in the source domain could enhance the performance of the ANN for automated IED classification. Here, as in the signal space analysis, two key conditions were examined: raw input without feature extraction (C3) and data with feature extraction (C4). The results provide critical insights into the benefits and limitations of the approach.

Initial analysis of raw source data (C3) revealed only a modest improvement in performance compared to raw signal space data. For the AND marking strategy, a slight increase was observed in sensitivity, but overall accuracy and specificity remained low. This was likely due to the significant data reduction inherent in projecting the multi-channel EEG onto a limited number of anatomical nodes. The simplified source model, particularly the fixed-orientation (1 parameter) projection, likely led to a loss of subtle, spatially distributed information critical for raw data classification. For the more heterogeneous OR marking strategy, performance

dropped even further. The free-orientation (3-parameter) model in this condition achieved a sensitivity of 0.66, which, while suggesting it could detect a wider range of IEDs, came at the cost of significantly lower accuracy and specificity. The performance differences between the fixed and free orientation models already hinted at the importance of retaining more dynamic information from the source. These findings highlighted the critical need for further feature enhancement when working with raw data.

Applying features to the source space data (C4) resulted in a notable improvement in ANN performance. Under the AND marking strategy, several feature sets achieved accuracies of 0.83 and 0.84 with balanced sensitivity and specificity, demonstrating that when combined with appropriate feature sets, 1 parameter projection can support reliable IED classification.

A key finding was the shift in feature dominance. While Katz FD (F2) was a top performer in signal space, statistical features (F1) became the most effective in 1-parameter projection, achieving an accuracy of 0.84. This change in utility is directly tied to the data representation. The source projection effectively suppresses background noise, leaving a clear, "peaky" IED waveform that is well captured by simple statistical measures. Conversely, the performance of F2 and other features sensitive to signal complexity dropped significantly. This is likely due to the 1-parameter compression of the simplified source model, which cannot account for dynamic properties such as a pattern's rotation or its propagation from the sulcal valley to the gyral crown, information that is essential for these features.

The benefit of a more complex source model was confirmed by the performance of the free-orientation (3-parameter) projection, where F2 performed better than in the fixed-orientation model. This demonstrates that allowing for more projection parameters retains more of the signal's complexity, which is crucial for features that rely on it. In contrast, the patch-based projection with fixed, redundant orientations failed to improve accuracy, as its lead field provided no additional benefit in modeling the data.

When applied to the OR marking strategy, performance with the feature remained lower than with AND marking. This highlights that the training data's consistency is paramount. The ambiguous and subjective nature of the OR-marked events introduced a variability that even feature extraction could not fully overcome.

In summary, the transition from signal to source space introduces a trade-off. While source projection provides spatial specificity and benefits from feature extraction, its overall performance did not surpass that of the signal space. The findings strongly suggest that to fully leverage the power of projection, a more complex

model with more projection parameters, such as a multi-location patch with flexible orientations, is required to better capture the dynamic nature of IEDs.

4.4 Comparison with previous research

The findings of this thesis aligned with existing research on automated interictal epileptiform discharge (IED) detection from EEG, particularly in the context of signal-space versus source-space representation and the role of feature extraction. This work builds upon the preliminary findings of Yeşilbaş et al., 2023.

The initial study by Yeşilbaş et al., 2023 demonstrated that a well-trained ANN can outperform expert markers in both sensitivity and specificity for IED detection. A key finding of their work was that feature extraction significantly improved ANN classification. This study also highlighted that Katz FD (F2) was the best single feature for representing spikes in both the AND-marking and the OR-marking datasets.

This thesis confirms that feature extraction is crucial for improving ANN performance in IED classification. However, it's been found that the dominance of features is dependent on the data representation. The finding extends the preliminary work by Yeşilbaş et al., 2023 and suggests that the utility of specific features is not universal but is highly sensitive to whether the data is presented in signal or source space. Analysis further explores the reasons for this shift, linking it to the information loss inherent in the process.

Several studies have explored the integration of source localization techniques such as beamforming, dipole fitting and minimum-norm estimation to extract spatially refined features for IED detection (Kaviri & Vinjamuri, 2024; Singh et al., 2022). These methods have been successfully employed to characterize cortical origins of epileptiform discharges through parameters like dipole location, orientation, and source waveform dynamics. Distributed beamforming techniques, by generating virtual sensor time series, permit the calculation of time-frequency and coherence measures that serve as robust features for classifying epileptiform discharges (Cheyne & Papanicolaou, 2015).

Kaviri and Vinjamuri, 2024; Singh et al., 2022 often utilizes more complex source models than the simplified ones in this thesis, typically involving many source locations and three waveforms per location to capture the full three-dimensional current flow. Our finding that the free orientation (3 parameter) model outperformed the fixed orientation (1 parameter) model directly supports this, highlighting the necessity of more projection parameters to effectively capture the dynamic and spatiotemporal complexity of the IED signals.

This thesis supports those findings by showing that source-localized features of both 1-parameter and 3-parameter projection can achieve reasonably strong classification performance, where the topographies remained stable from onset to the half of the rising flank. However, if the pattern rotates, a fixed-orientation strategy would not be sufficient. The improvement observed when applying feature extraction in source space over raw input data is consistent with studies showing that features improve the sensitivity and spatial specificity necessary for reliable IED detection (Zhang, 2015). Furthermore, the use of spectral measures, such as those computed from PSD in specific bands, reflects a broader trend in the literature where wavelet transforms, multi-taper spectral analysis, and coherence measures are used to isolate oscillatory dynamics typical of IEDs (Iravani, 2021; Zheng et al., 2021).

However, this study highlights that not all features generalize equally well across domains as well. Katz FD, which performed well in signal space, showed a decrease in accuracy when applied to 1-parameter-source-space-projection. This observation aligns with challenges reported in prior studies when applying certain nonlinear or complexity-based features to noise-sensitive data (Shirani et al., 2024). Such findings suggest that while source localization provides anatomical specificity, it may reduce the power of some features.

Some studies have also applied this deep learning approach to the source localized EEG, showing that raw source time series can improve classification due to their enhanced spatial resolution (Kaviri & Vinjamuri, 2024). These deep learning models benefit from the spatial specificity offered by source localization while also retaining the ability to learn complex signals across space and time (Zhang, 2015).

In summary, the literature strongly supports both feature-based and deep learning strategies for IED detection. This study contributes to that body of work by offering a direct condition-wise comparison of signal space versus source space, both with and without feature extraction.

4.5 Clinical Implications

The findings of this thesis have important clinical implications for the automated detection of IEDs in epilepsy management. The high accuracy achieved by ANN using feature-extracted EEG data in signal space suggests strong potential for developing assistive tools that could support epileptologists. Automated IED detection systems could lead to several benefits, such as enhanced diagnostic efficiency, improved diagnostic consistency, facilitated long-term monitoring and guided treatment decisions.

While source space analysis did not universally outperform signal space, its abil-

ity to localize the activity to anatomical brain regions holds promise for evaluation. Further development in this area could lead to tools that not only detect IEDs but also provide clinically relevant spatial information for presurgical evaluation or treatment planning.

It is also important to consider the balance between sensitivity and specificity in clinical use. A tool optimized for high sensitivity, reliably detecting the majority of potential IEDs, may still be valuable even if specificity is lower. In such a workflow, the automated system would act as a broad screening tool, ensuring that few or no events are missed, while the clinician applies their expertise to review and exclude false positives. From this perspective, models that exhibit high sensitivity but lower specificity could still meaningfully support clinical decision-making by reducing the chance of missed epileptiform activity.

4.6 Limitations and Future work

Despite the results, this study has further limitations that provide valuable directions for future research.

First, the dataset was restricted to a single patient. While this allowed for systematic evaluation within a controlled setting, it limits the generalization of the findings. To ensure the robustness and clinical applicability, future studies should include larger datasets spanning multiple patients with diverse epilepsy types and IED characteristics. This would allow the trained models to be validated across a broader spectrum of clinical presentations.

Second, the source space analysis relied on a 1-parameter source projection, i.e., a single dipole waveform per location. This simplification may have reduced the capacity of certain features, such as Katz FD, to capture discriminative patterns. Extending the model to incorporate more complex representations could better preserve the spatiotemporal dynamics of IEDs.

Third, although free orientation was tested, it remained constrained to a single dipole per source. More realistic anatomical models, such as allowing multi-path configurations spanning sulcal and gyral regions, may provide richer information and improve classification accuracy. Such an approach could also reflect the physiological spread of epileptic activity.

Also, investigating the impact of different source analysis methods on ANN accuracy, potentially leading to improved classification and better polarity insights into the spatial representation of IEDs.

Finally, some features exhibited strong representation dependence, performing well in signal space but not in source space. This suggests that the interaction be-

tween preprocessing, source reconstruction and feature extraction should be examined more systematically, potentially leading to optimized pipelines for automated IED detection.

4.7 Conclusion

This thesis systematically explored the impact of different EEG data conditions both in signal and source space and used ANN for identifying IEDs. The results clearly demonstrate that raw EEG data alone lacks the structure required for accurate classification, while the application of feature extraction significantly enhances model performance, especially in signal space. Although source localization offers anatomical insights, its integration with feature-based approaches gave only modest improvements. This limitation is likely linked to the use of a 1-parameter source projection, which restricts the amount of preserved information. Even though 3-parameter source projection has been tested, increasing the degrees of freedom may better balance anatomical specificity with classification accuracy.

The findings reinforce the importance of carefully choosing data representations and feature sets in EEG-based classification tasks. In clinical settings, automated IED detection tools built on such frameworks could support neurologists by improving diagnostic efficiency and consistency. Future work should expand analyses to multi-patient datasets, evaluate richer source localization strategies with greater parameter flexibility, and explore advanced deep learning architectures to further enhance the robustness and clinical value of automated detection tools.

References

Aanestad, E., Gilhus, N. E., Olberg, H. K., Kural, M. A., Beniczky, S., & Brogger, J. (2023). Spike count and morphology in the classification of epileptiform discharges. *Frontiers in Neurology*, *14*, 1165592. https://doi.org/10.3389/fneur.2023.1165592

Abdalla, O. A. (2011). *Proposed methodology for optimizing the training parameters of a multilayer feed-forward artificial neural networks using a genetic algorithm* [PhD Thesis]. Universiti Teknologi PETRONAS.

Abraham, A. (2005). Artificial neural networks [Part 8. Elements: B—Signal Conditioning, 3. AI Signal Processing Techniques]. In P. H. Sydenham & R. Thorn (Eds.), *Handbook of measuring system design* (Vol. 3). Wiley. https://doi.org/10.1002/0471497398.mm421

Agatonovic-Kustrin, S., & Beresford, R. (2000). Basic concepts of artificial neural network (ann) modeling and its application in pharmaceutical research. *Journal of Pharmaceutical and Biomedical Analysis*, *22*(5), 717–727. https://doi.org/10.1016/S0731-7085(99)00272-1

Akter, M. S., Islam, M. R., Iimura, Y., Sugano, H., Fukumori, K., Wang, D., Tanaka, T., & Cichocki, A. (2020). Multiband entropy-based feature-extraction method for automatic identification of epileptic focus based on high-frequency components in interictal ieeg. *Scientific Reports*, *10*(1), 7044.

Ameera, A., A., S., & Ibrahim, Z. (2019). Analysis of eeg spectrum bands using power spectral density for pleasure and displeasure state. *IOP Conference Series: Materials Science and Engineering*, *557*, 012030. https://doi.org/10.1088/1757-899X/557/1/012030

Aminoff, M. J. (2012). Chapter 3 - electroencephalography: General principles and clinical applications. In M. J. Aminoff (Ed.), *Aminoff's electrodiagnosis in clinical neurology (sixth edition)* (Sixth Edition, pp. 37–84). W.B. Saunders. https://doi.org/10.1016/B978-1-4557-0308-1.00003-0

Antonakakis, M., Kaiser, F., Rampp, S., Kovac, S., Wiendl, H., Stummer, W., Gross, J., Kellinghaus, C., Khaleghi-Ghadiri, M., Möddel, G., & Wolters, C. H. (2024). Targeted and optimized multi-channel transcranial direct current stimulation for focal epilepsy: An n-of-1 trial. *Brain Stimulation*, *17*, 221–223. https://doi.org/10.1016/j.brs.2024.02.010

Aydin, Ü., Rampp, S., Wollbrink, A., Kugel, H., Cho, J.-H., Knösche, T. R., Grova, C., Wellmer, J., & Wolters, C. H. (2017). Zoomed MRI guided by combined EEG/MEG source analysis: A multimodal approach for optimizing presurgi-

cal epilepsy work-up and its application in a multi-focal epilepsy patient case study. *Brain Topography*, *30*(4), 417–433. https://doi.org/10.1007/s10548-017-0568-9

Aydin, Ü., Vorwerk, J., Dümpelmann, M., Küpper, P., Kugel, H., Heers, M., Wellmer, J., Kellinghaus, C., Haueisen, J., Rampp, S., Stefan, H., & Wolters, C. H. (2015). Combined EEG/MEG can outperform single modality EEG or MEG source reconstruction in presurgical epilepsy diagnosis. *PLOS ONE*, *10*(3), e0118753. https://doi.org/10.1371/journal.pone.0118753

Barzegaran, E., & Knyazeva, M. G. (2017). Functional connectivity analysis in eeg source space: The choice of method. *PLOS ONE*, *12*(7), e0181105. https://doi.org/10.1371/journal.pone.0181105

Bekhti, Y. (2018). *Contributions to sparse source localization for meg/eeg brain imaging* [PhD thesis]. Télécom ParisTech [NNT: 2018ENST0017]. https://theses.hal.science/tel-03409068

Benbadis, S. (2009). The differential diagnosis of epilepsy: A critical review. *Epilepsy Behavior*, *15*, 15–21. https://doi.org/10.1016/j.yebeh.2009.02.024

Beutel, J., Fitzpatrick, J. M., Horii, S. C., Kim, Y., Kundel, H. L., Sonka, M., & Van Metter, R. L. (2000). *Handbook of medical imaging. volume 1: Physics and psychophysics*. SPIE Optical Engineering Press.

Boonyakitanont, P., Lek-uthai, A., Chomtho, K., & Songsiri, J. (2020). A review of feature extraction and performance evaluation in epileptic seizure detection using eeg. *Biomedical Signal Processing and Control*, *57*, 101702. https://doi.org/10.1016/j.bspc.2019.101702

Boubchir, L., Daachi, B., & Pangracious, V. (2017). A review of feature extraction for eeg epileptic seizure detection and classification. *2017 40th International Conference on Telecommunications and Signal Processing (TSP)*, 456–460. https://doi.org/10.1109/TSP.2017.8076027

Brette, R., & Destexhe, A. (Eds.). (2012). *Handbook of neural activity measurement*. Cambridge University Press. https://doi.org/10.1017/CBO9780511979958

Çetin, V., & Yıldız, O. (2022). A comprehensive review on data preprocessing techniques in data analysis. *Pamukkale University Journal of Engineering Sciences*, *28*(2), 299–312. https://doi.org/10.5505/pajes.2021.62687

Cetişli, B., & Barkana, A. (2010). Speeding up the scaled conjugate gradient algorithm and its application in neuro-fuzzy classifier training. *Soft Computing*, *14*(4), 365–378. https://doi.org/10.1007/s00500-009-0410-8

Chawla, N. V., Bowyer, K. W., Hall, L. O., & Kegelmeyer, W. P. (2002). Smote: Synthetic minority over-sampling technique. *Journal of Artificial Intelligence Research*, *16*, 321–357.

Cheyne, D. O., & Papanicolaou, A. C. (2015). Magnetoencephalography and magnetic source imaging [Functional Brain Imaging in Cognitive Neurosciences and Neuropsychology]. In A. C. Papanicolaou (Ed.), *Functional brain imaging in cognitive neurosciences and neuropsychology*. Oxford University Press.

de Moraes, F. D., & Callegari, D. A. (2014). *Automated detection of interictal spikes in eeg: A literature review* (tech. rep.). Pontifícia Universidade Católica do Rio Grande do Sul. Av. Ipiranga, 6681 - Porto Alegre/RS, Brasil.

Doschoris, M., & Kariotou, F. (2017). Mathematical foundation of electroencephalography. In P. Sittiprapaporn (Ed.), *Electroencephalography*. IntechOpen. https://doi.org/10.5772/68021

Fisher, R. S., Acevedo, C., Arzimanoglou, A., Bogacz, A., Cross, J. H., Elger, C. E., Engel, J., Forsgren, L., French, J. A., Glynn, M., Hesdorffer, D. C., Lee, B., Mathern, G. W., Moshé, S. L., Perucca, E., Scheffer, I. E., Tomson, T., Watanabe, M., & Wiebe, S. (2014). ILAE Official Report: A practical clinical definition of epilepsy. *Epilepsia*, *55*(4), 475–482. https://doi.org/10.1111/epi.12550

Forjaco Jorge, J. P. (2016). *Simultaneous eeg-fmri at ultra-high field for the study of human brain function* [PhD Thesis]. École Polytechnique Fédérale de Lausanne (EPFL). https://doi.org/10.5075/epfl-thesis-6969

Fuchs, M., Kastner, J., Wagner, M., Hawes, S., & Ebersole, J. S. (2002). A standardized boundary element method volume conductor model. *Clinical Neurophysiology*, *113*(5), 702–712. https://doi.org/10.1016/s1388-2457(02)00030-5

Gramfort, A., Papadopoulo, T., Olivi, E., & Clerc, M. (2010). Openmeeg: Open source software for quasistatic bioelectromagnetics. *BioMedical Engineering OnLine*, *9*(1), 45. https://doi.org/10.1186/1475-925X-9-45

Guilhoto, L. F. (2018). An overview of artificial neural networks for mathematicians [University of Chicago Mathematics REU Program].

Güven, A., Altınkaynak, M., Dolu, N., Izzetoglu, M., pektaş, F., Özmen, S., Demirci, E., & Batbat, T. (2020). Combining functional near-infrared spectroscopy and eeg measurements for the diagnosis of attention-deficit hyperactivity disorder. *Neural Computing and Applications*, *32*. https://doi.org/10.1007/s00521-019-04294-7

Hinrichs, H., Scholz, M., Baum, A. K., et al. (2020). Comparison between a wireless dry electrode eeg system with a conventional wired wet electrode eeg system

for clinical applications. *Scientific Reports*, *10*, 5218. https://doi.org/10.1038/s41598-020-62154-0

Holleman, J., Zhang, F., & Otis, B. (2011). Spike detection and characterization. In *Ultra low-power integrated circuit design for wireless neural interfaces* (pp. 51–63). Springer New York. https://doi.org/10.1007/978-1-4419-6727-5_7

Höltershinken, M. B., Lange, P., Erdbrügger, T., Buschermöhle, Y., Wallois, F., Buyx, A., Pursiainen, S., Vorwerk, J., Engwer, C., & Wolters, C. H. (2025). The local subtraction approach for eeg and meg forward modeling. *SIAM Journal on Scientific Computing*, *47*(1), B160–B189. https://doi.org/10.1137/23M1582874

Hussein, A. F., Arunkumar, N., Gomes, C., Alzubaidi, A. K., Habash, Q. A., Santamaria-Granados, L., Mendoza-Moreno, J. F., & Ramirez-Gonzalez, G. (2018). Focal and Non-Focal Epilepsy Localization: A Review. *IEEE Access*, *6*, 49306–49324. https://doi.org/10.1109/ACCESS.2018.2867078

Iravani, B. (2021). *Novel measure of olfactory bulb function in health and disease* [PhD Thesis]. Karolinska Institutet [Printed by US-AB]. Karolinska Institutet.

Jatoi, M. A., Kamel, N., Malik, A. S., Faye, I., & Begum, T. (2014). A survey of methods used for source localization using eeg signals. *Biomedical Signal Processing and Control*, *11*, 42–52. https://doi.org/10.1016/j.bspc.2014.01.009

Karoly, P. J., Freestone, D. R., Boston, R., Grayden, D. B., Himes, D., Leyde, K., Seneviratne, U., Berkovic, S., O'Brien, T., & Cook, M. J. (2016). Interictal spikes and epileptic seizures: Their relationship and underlying rhythmicity. *Brain*, *139*(4), 1066–1078. https://doi.org/10.1093/brain/aww019

Kaviri, S. M., & Vinjamuri, R. (2024). Integrating electroencephalography source localization and residual convolutional neural network for advanced stroke rehabilitation [Article 967]. *Bioengineering*, *11*(10), 967. https://doi.org/10.3390/bioengineering11100967

Kavzoglu, T. (2001). An investigation of the design and use of feed-forward artificial neural networks in the classification of remotely sensed images. *Computers & Geosciences*, *27*(3), 361–372. https://doi.org/10.1016/S0098-3004(00)00141-7

Kim, K. H., & Kim, S. (2000). Neural spike sorting under nearly 0-db signal-to-noise ratio using nonlinear energy operator and artificial neural-network classifier.

IEEE Transactions on Biomedical Engineering, *47*, 1406–1411. https://doi.org/10.1109/10.871415

Kirsch, H. E., Robinson, S. E., Mantle, M., & Nagarajan, S. (2006). Automated localization of magnetoencephalographic interictal spikes by adaptive spatial filtering. *Clinical Neurophysiology*, *117*(10), 2264–2271. https://doi.org/10.1016/j.clinph.2006.06.708

Kordos, M., & Duch, W. (2008). Variable step search algorithm for feedforward networks [Artificial Neural Networks (ICANN 2006) / Engineering of Intelligent Systems (ICEIS 2006)]. *Neurocomputing*, *71*(13), 2470–2480. https://doi.org/10.1016/j.neucom.2008.02.019

Kumar, P., & Upadhyay, P. K. (2025). A hybrid optimization-enhanced 1d-rescnn framework for epileptic spike detection in scalp eeg signals. *Scientific Reports*, *15*(1), 5707. https://doi.org/10.1038/s41598-025-90164-3

Kybic, J., Clerc, M., Abboud, T., Faugeras, O., Keriven, R., & Papadopoulo, T. (2005). A common formalism for the integral formulations of the forward eeg problem. *IEEE Transactions on Medical Imaging*, *24*(1), 12–28. https://doi.org/10.1109/TMI.2004.837363

Lantz, G., Spinelli, L., Seeck, M., de Peralta Menendez, R. G., Sottas, C. C., & Michel, C. M. (2003). Propagation of interictal epileptiform activity can lead to erroneous source localizations: A 128-channel eeg mapping study. *Journal of Clinical Neurophysiology*, *20*(5), 311–319. https://doi.org/10.1097/00004691-200309000-00003

Larsson, C. (2018). Chapter 4 - self-similarity, fractality, and chaos. In *5g networks* (pp. 67–102). Academic Press. https://doi.org/10.1016/B978-0-12-812707-0.00009-7

Lehnertz, K. (2008). Epilepsy and nonlinear dynamics [Epub 2008 Jul 9]. *Journal of Biological Physics*, *34*(3-4), 253–266. https://doi.org/10.1007/s10867-008-9090-3

Ma, W., Zheng, Y., Li, T., Li, Z., Li, Y., & Wang, L. (2024). A comprehensive review of deep learning in eeg-based emotion recognition: Classifications, trends, and practical implications. *PeerJ Computer Science*, *10*, e2065. https://doi.org/10.7717/peerj-cs.2065

Makkonen, M. (2023). *Real-time electroencephalography-based spike detection for suppression of epileptogenic activity with transcranial magnetic stimulation* [Master's Thesis]. Aalto University, School of Science.

Mecarelli, O. (2019). Electrode Placement Systems and Montages. In O. Mecarelli (Ed.), *Clinical Electroencephalography* (pp. 35–52). Springer International Publishing. https://doi.org/10.1007/978-3-030-04573-9_4

Michel, C. M., Murray, M. M., Lantz, G., Gonzalez, S., Spinelli, L., & Peralta, R. G. D. (2004). Eeg source imaging. *Clinical Neurophysiology*, *115*, 2195–2222. https://doi.org/10.1016/j.clinph.2004.06.001

Milligan, T. A. (2021). Epilepsy: A Clinical Overview. *The American Journal of Medicine*, *134*(7), 840–847. https://doi.org/10.1016/j.amjmed.2021.01.038

Myers, M. H., Padmanabha, A., Bidelman, G. M., & Wheless, J. W. (2020). Seizure localization using eeg analytical signals. *Clinical Neurophysiology*, *131*(9), 2131–2139. https://doi.org/10.1016/j.clinph.2020.05.034

Noachtar, S., Binnie, C., Ebersole, J., Mauguière, F., Sakamoto, A., & Westmoreland, B. (1999). A glossary of terms most commonly used by clinical electroencephalographers and proposal for the report form for the eeg findings. the international federation of clinical neurophysiology. *Electroencephalography and Clinical Neurophysiology. Supplement*, *52*, 21–41. https://doi.org/10.1055/s-2003-812583

Noachtar, S., & Rémi, J. (2009). The role of eeg in epilepsy: A critical review. *Epilepsy & Behavior*, *15*(1), 22–33. https://doi.org/10.1016/j.yebeh.2009.02.035

Nunes, V. D., Sawyer, L., Neilson, J., Sarri, G., & Cross, J. H. (2012). Diagnosis and management of the epilepsies in adults and children: Summary of updated NICE guidance. *BMJ*, *344*, e281–e281. https://doi.org/10.1136/bmj.e281

Oostenveld, R., Fries, P., Maris, E., & Schoffelen, J.-M. (2011). Fieldtrip: Open source software for advanced analysis of meg, eeg, and invasive electrophysiological data. *Computational Intelligence and Neuroscience*, *2011*, 1–9. https://doi.org/10.1155/2011/156869

P.A., C., & Desai, S. S. (2023). *Effective epileptic seizure detection by classifying focal and non-focal eeg signals using human learning optimization-based hidden markov model*.

Pattanayak, S., Singh, T., Kumar, R., et al. (2024, September). Prognosis of pathological complete response to neoadjuvant chemotherapy in breast cancer using dce-mri and inceptionv3 [Preprint (Version 1) available at Research Square]. https://doi.org/10.21203/rs.3.rs-4938587/v1

Paul, B., & Karn, B. (2023). Heart disease prediction using scaled conjugate gradient backpropagation of artificial neural network. *Soft Computing*, *27*(11), 6687–6702. https://doi.org/10.1007/s00500-022-07649-w

Raju, V. N. G., Lakshmi, K. P., Jain, V. M., Kalidindi, A., & Padma, V. (2020). Study the influence of normalization/transformation process on the accuracy of supervised classification. *2020 Third International Conference on Smart Systems and Inventive Technology (ICSSIT)*, 729–735. https://doi.org/10.1109/ICSSIT48917.2020.9214160

Ramakrishnan, S., Asuncion, R. M. D., & Rayi, A. (2025, January). Localization-related epilepsies on eeg [[Updated 2024 Apr 30]]. In *Statpearls [internet]*. StatPearls Publishing. https://www.ncbi.nlm.nih.gov/books/NBK557645/

Ramantani, G. (2018). *Contribution des sources épileptiques inter-critiques et critiques à l'eeg de scalp* [PhD Thesis]. Université de Lorraine [Thèse présentée à l'Ecole Doctorale BioSE (Biologie-Santé-Environnement)].

Rampp, S., Stefan, H., Wu, X., Kaltenhäuser, M., Maess, B., Schmitt, F. C., Wolters, C. H., Hamer, H., Kasper, B. S., Schwab, S., Doerfler, A., Blümcke, I., Rössler, K., & Buchfelder, M. (2019). Magnetoencephalography for epileptic focus localization in a series of 1000 cases. *Brain*, *142*(10), 3059–3071. https://doi.org/10.1093/brain/awz231

Rosenow, F., & Lüders, H. (2001). Presurgical evaluation of epilepsy. *Brain*, *124*(9), 1683–1700. https://doi.org/10.1093/brain/124.9.1683

Rousseau, R., Egghe, L., & Guns, R. (2018). Chapter 4 - statistics. In *Becoming metric-wise* (pp. 67–97). Chandos Publishing. https://doi.org/10.1016/B978-0-08-102474-4.00004-2

Rüdisüli, M., Schildhauer, T. J., Biollaz, S. M. A., & Van Ommen, J. R. (2013). Measurement, monitoring and control of fluidized bed combustion and gasification. In F. Scala (Ed.), *Fluidized bed technologies for near-zero emission combustion and gasification* (pp. 813–864). Woodhead Publishing. https://doi.org/10.1533/9780857098801.3.813

Ruiz de Miras, J. (2016, August). Fractal analysis in matlab: A tutorial for neuroscientists. In A. Di Ieva (Ed.), *The fractal geometry of the brain* (pp. 523–532). Springer. https://doi.org/10.1007/978-1-4939-3995-4_33

Sanei, S., & Chambers, J. (2007). Brain–computer interfacing. In *Eeg signal processing* (pp. 239–265). John Wiley; Sons, Ltd. https://doi.org/10.1002/9780470511923.ch7

Sarmast, S. T., Abdullahi, A. M., & Jahan, N. (2020). Current Classification of Seizures and Epilepsies: Scope, Limitations and Recommendations for Future Action. *Cureus*. https://doi.org/10.7759/cureus.10549

Shaaban, S., Al-Beltagi, M., El Rashidy, O., Nassar, M., & El Gendy, Y. (2023). Ketogenic diet in childhood epilepsy: Clinical algorithm in a tertiary care

center. *Frontiers in Pediatrics*, *11*, 1221781. https://doi.org/10.3389/fped.2023.1221781

Shirani, S., Abdi-Sargezeh, B., Valentin, A., Alarcon, G., Jarchi, D., Bird, J., & Sanei, S. (2024). Distributed beamforming for localization of brain seizure sources from intracranial eeg array. *2024 32nd European Signal Processing Conference (EUSIPCO)*, 1117–1121. https://doi.org/10.23919/EUSIPCO63174.2024.10715203

Simbun, A., & Kumar, S. (2025). Artificial intelligence-driven prognostic classification of covid-19 using chest x-rays: A deep learning approach [Preprint available on arXiv]. https://arxiv.org/abs/2503.13277

Singh, J., Ebersole, J. S., & Brinkmann, B. H. (2022). From theory to practical fundamentals of electroencephalographic source imaging in localizing the epileptogenic zone. *Epilepsia*, *63*(10), 2476–2490. https://doi.org/10.1111/epi.17361

Smith, S. J. (2005). Eeg in the diagnosis, classification, and management of patients with epilepsy. *Journal of Neurology, Neurosurgery & Psychiatry*, *76*, ii2–ii7. https://doi.org/10.1136/jnnp.2005.069245

St. Louis, E., Frey, L., Britton, J., Hopp, J., Korb, P., Koubeissi, M., Lievens, W., & Elia. (2016). *Electroencephalography (EEG): An Introductory Text and Atlas of Normal and Abnormal Findings in Adults, Children, and Infants*. American Epilepsy Society. https://doi.org/10.5698/978-0-9979756-0-4

The MathWorks, I. (2023a). Deep learning toolbox. https://www.mathworks.com/products/deep-learning.html

The MathWorks, I. (2023b). Signal processing toolbox. https://www.mathworks.com/products/deep-learning.html

The MathWorks, I. (2023c). Statistics and machine learning toolbox. https://www.mathworks.com/products/deep-learning.html

Uyulan, C., Ergüzel, T. T., & Tarhan, N. (2019). Entropy-based feature extraction technique in conjunction with wavelet packet transform for multi-mental task classification. *Biomedical Engineering / Biomedizinische Technik*, *64*(5), 529–542. https://doi.org/10.1515/bmt-2018-0105

van de Steen, F., Faes, L., Karahan, E., Songsiri, J., Valdes Sosa, P. A., & Marinazzo, D. (2016). Critical comments on eeg sensor space dynamical connectivity analysis [arXiv preprint arXiv:1607.03687]. https://doi.org/10.48550/arXiv.1607.03687

Vulliemoz, S. (2012). *Functional imaging of epileptic activity in humans* [Privatdocent Thesis]. University of Geneva. https://doi.org/10.13097/archive-ouverte/unige:23178

Wang, L., & Carvalho, L. (2024). Multiclass roc [Preprint available on arXiv]. https://arxiv.org/abs/2404.13147

Wang, L., Xue, W., Li, Y., Luo, M., Huang, J., Cui, W., & Huang, C. (2017). Automatic epileptic seizure detection in eeg signals using multi-domain feature extraction and nonlinear analysis. *Entropy*, *19*(6), 222. https://doi.org/10.3390/e19060222

Wolters, C., & Munck, J. C. d. (2007). Volume conduction [revision #137330]. *Scholarpedia*, *2*(3), 1738. https://doi.org/10.4249/scholarpedia.1738

World Health Organization. (2022). *Epilepsy*. https://www.who.int/news-room/fact-sheets/detail/epilepsy

Yeşilbaş, D., Melnik, S., Rampp, S., Kellinghaus, C., Kovac, S., Möddel, G., Güven, A., Batbat, T., & Wolters, C. H. (2023). Comparison of feature extraction methods for spike detection with artificial neural networks: A focal epilepsy case study [Poster presentation]. *57th DGBMT Annual Conference on Biomedical Engineering (DGBMT2023)*. https://www.sci.utah.edu/~wolters/PaperWolters/2023/YesilbasEtAl_BMT2023_Poster.pdf

Zhang, H. (2015, June). *Multimodal functional neuroimaging of epilepsy and pain* [PhD Dissertation]. University of Minnesota. https://conservancy.umn.edu/handle/11299/174806

Zhao, D., Wang, Y., Wang, Q., & Wang, X. (2019). Comparative analysis of different characteristics of automatic sleep stages. *Computer Methods and Programs in Biomedicine*, *175*, 53–72. https://doi.org/10.1016/j.cmpb.2019.04.004

Zheng, L., Sheng, J., Cen, Z., Teng, P., Wang, J., Wang, Q., Lee, R. R., Luan, G., Huang, M., & Gao, J.-H. (2021). Enhanced fast-vestal for magnetoencephalography source imaging: From theory to clinical application in epilepsy. *IEEE Transactions on Biomedical Engineering*, *68*(3), 793–806. https://doi.org/10.1109/TBME.2020.3016468